PYROLYSIS AND IGNITION BEHAVIOR OF COAL, CATTLE BIOMASS, AND COAL/CATTLE BIOMASS BLENDS

A Thesis

by

BRANDON RAY MARTIN

Submitted to the Office of Graduate Studies of
Texas A&M University
in partial fulfillment of the requirements for the degree of

MASTER OF SCIENCE

December 2006

Major Subject: Mechanical Engineering

PYROLYSIS AND IGNITION BEHAVIOR OF COAL, CATTLE BIOMASS, AND COAL/CATTLE BIOMASS BLENDS

A Thesis

by

BRANDON RAY MARTIN

Submitted to the Office of Graduate Studies of
Texas A&M University
in partial fulfillment of the requirements for the degree of

MASTER OF SCIENCE

Approved by:

Chair of Committee,	Kalyan Annamalai
Committee Members,	Jerald Caton
	Saqib Mukhtar
Head of Department,	Dennis O'Neal

December 2006

Major Subject: Mechanical Engineering

ABSTRACT

Pyrolysis and Ignition Behavior of Coal, Cattle Biomass, and Coal/Cattle Biomass Blends. (December 2006)

Brandon Ray Martin, B.S., University of Arkansas

Chair of Advisory Committee: Dr. Kalyan Annamalai

Increases in demand, lower emission standards, and reduced fuel supplies have fueled the recent effort to find new and better fuels to power the necessary equipment for society's needs. Often, the fuels chosen for research are renewable fuels derived from biomass. Current research at Texas A&M University is focused on the effectiveness of using cattle manure biomass as a fuel source in conjunction with coal burning utilities. The scope of this project includes fuel property analysis, pyrolysis and ignition behavior characteristics, combustion modeling, emissions modeling, small scale combustion experiments, pilot scale commercial combustion experiments, and cost analysis of the fuel usage for both feedlot biomass and dairy biomass. This paper focuses on fuel property analysis and pyrolysis and ignition characteristics of feedlot biomass. Deliverables include a proximate and ultimate analysis, pyrolysis kinetics values, and ignition temperatures of four types of feedlot biomass (low ash raw manure [LARM], low ash partially composted manure [LAPC], high ash raw manure [HARM], and high ash partially composted manure [HAPC]) as well as blends of each biomass with Texas lignite coal (TXL). Activation energy results for pure samples of each fuel using the

single reaction model rigorous solution were as follows: 45 kJ/mol (LARM), 43 kJ/mol (LAPC), 38 kJ/mol (HARM), 36 kJ/mol (HAPC), and 22 kJ/mol (TXL). Using the distributed activation energy model the activation energies were 169 kJ/mol (LARM), 175 kJ/mol (LAPC), 172 kJ/mol (HARM), 173 kJ/mol (HAPC), and 225 kJ/mol (TXL). Ignition temperature results for pure samples of each of the fuels were as follows: 734 K (LARM), 745 K (LAPC), 727 (HARM), 744 K (HAPC), and 592 K (TXL). There was little difference observed between the ignition temperatures of the 50% blends of coal with biomass and the pure samples of coal as observed by the following results: 606 K (LARM), 571 K (LAPC), 595 K (HARM), and 582 K (HAPC).

ACKNOWLEDGEMENTS

This work is supported by a grant from the Texas Commission on Environmental Quality Grant # 582-5-65591 0015 and the US-DOE grant # DE-FG36-05GO85003 through the Texas Engineering Experiment Station, Texas A&M University. Special thanks to Dr. John Sweeten and Kevin Heflin for providing and preparing fuel samples, to the research team at the Renewable Energy Lab at Texas A&M University, to the members of my committee, and to my Advisor, Dr. Kalyan Annamalai. I would also like to thank my wife, Elizabeth, for her help and patience during busy working days. Finally, I would like to thank God for his provision and blessings over the past year.

TABLE OF CONTENTS

Page

CHAPTER Page

LIST OF FIGURES

Page

Page

Page

LIST OF TABLES

Page

ACRONYMS

AWDF ..... Animal Waste Derived Biomass Fuels
CB..... Cattle biomass
CO_2 ..... Carbon Dioxide
DAF ..... Dry Ash Free
DB ..... Dairy Biomass
DOE..... Department of Energy
DSC ..... Differential Scanning Calorimeter
EPA ..... Environmental Protection Agency
FB ..... Feedlot biomass (Cattle manure or Cattle Biomass CB)
FC ..... Fixed Carbon
GRA ..... Graduate Research Assistant
HARM..... High Ash Feedlot Biomass Raw form
HAPC ..... High Ash Feedlot Biomass Partially Composted
HHV ..... Higher Heating Value
HV ..... Heating value
LARM ..... Low Ash Feedlot Biomass
LAPC..... Low Ash Feedlot Biomass Partially Composted
mmBTU..... million BTU
N2 ..... Nitrogen
NOx ..... Oxides of Nitrogen
O2 ..... Oxygen
RM..... Raw Manure
S..... Sulfur
TAMU ..... Texas A&M University
TAES ..... Texas Agricultural Extension Service
TGA..... Thermo-Gravimetric Analysis
TXU..... Texas Utilities
USDA ..... US Dept of Agriculture
VM ..... Volatile matter

CHAPTER I

INTRODUCTION

Biomass fuel research has attracted a lot of attention in recent years due to growing energy needs and shrinking fossil fuel supplies. These combined factors have led to increased cost for utility consumers in the US since 71% of electric power is generated form fossil fuel power plants, see figure I.1 for details. As a result, many new renewable fuel sources or renewable fuel technologies are becoming economically competitive and are under consideration. These include biomass derived from plant matter such as wood, corn stalks, and sugar cane as well as animal by-products such as manure and waste carcasses.

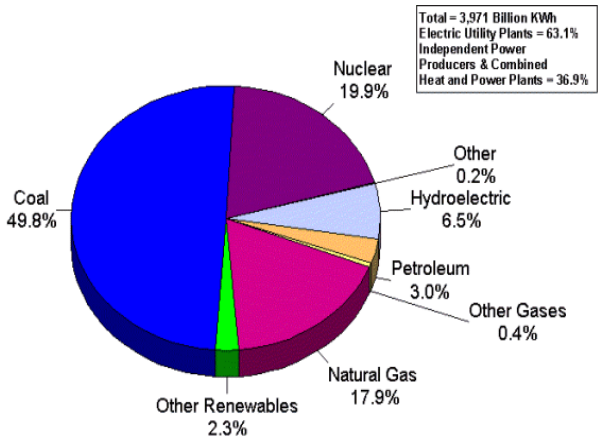

Figure I.1: Electric Power Generation by Fuel Type (2004)
Source: US Department of Energy website, www.energy.gov

A second driving force behind the research into renewable energy sources is the need to meet future emissions standards. Greenhouse gas regulation is under debate in

---

This thesis follows the style of Fuel.

the US, with the US Supreme Court hearing a case to determine if CO_2 emissions can be regulated under the Clean Air Act of 1990. Unlike fossil fuels, biomass fuels are near CO_2 neutral fuels (net CO_2 released is near zero). The majority of CO_2 released during combustion comes from plants and is reabsorbed by plants. Biomass fuels have also been shown to have emissions control properties for NO_x and SO_x emissions. Emission reduction potential depends on fuel characteristics; for animal waste fuels NO_x reduction is due to the amount of urea present in the fuel.

Current research at Texas A&M University is focused on cattle biomass (CB) potential as an auxiliary fuel in several applications: co-fired with coal in a utility application, used in the re-burn section of a coal power plant, and as primary or co-fired fuel for gasification. There are two types of CB being studied: feedlot biomass (FB) from Amarillo, TX and dairy biomass (DB) from farms Northwest of Waco, TX. This work focuses on the pyrolysis and ignition characteristics of FB related to modeling biomass fuels during pyrolysis, ignition, and combustion. The four types of feedlot biomass being tested are HAPC (High Ash Partially Composted), LAPC (Low Ash Partially Composted), HARM (High Ash Raw Manure), and LARM (Low Ash Raw Manure). High ash manure was collected from soil surfaced feedlots, while low ash biomass was collected from fly ash surfaced feedlots. The manure was collected from feedlots at the end of a 90-180 day feeding cycle and then divided into two categories, raw and partially composted manure. Raw manure was taken from pens, dried, and ground for use in the laboratory furnace. Partially composted manure was composted over a period of 3-4 months to homogenize the fuel properties, then dried and ground.

CHAPTER II

LITERATURE REVIEW

II.1 Chapter Overview

The literature review gives a brief summary of the previous and current work found in literature in coal / biomass fuel characterization. First, the collection techniques for cattle manure biomass are discussed to show how fuel properties are affected. Next, the properties of the different types of biomass currently being studied are compared with coal. An account of pyrolysis and ignition modeling of many biomass fuels are then described. The last section explains the scope of this research and how it furthers this field of study.

II.2 Manure Collection Techniques

Feedlot biomass fuel properties (chiefly ash content) depend greatly on the collection technique used when the manure is gathered from the feedlots; this is due in large part to the surface of the feedlot. Most feedlots have a soil base with an interfacial layer which consists of mixed soil and manure. If the manure is not harvested carefully some of the interfacial layer will be disturbed or collected with the manure. This leads to higher ash content in the manure. Collection techniques vary between feedlots but usually one of the following methods is used: wheel loader alone, chisel-plow followed by wheel loader, and elevating scraper [1], see figure II.1.

A. Wheel Loader B. Chisel Plow C. Elevating Scraper

Figure II.1: Manure collection equipment

The first manure harvesting method is to use a wheel loader to scrape and collect the manure from the surface of the feedlot. However, this is not the most effective method since wheel loaders can easily damage the interfacial layer. The quality of the collected manure depends greatly on the skill of the operator. A more efficient technique (tons/hour) is to use a chisel-plow to loosen the manure and then collect the manure with the wheel loader. Again, this method can easily damage the interfacial layer. Another disadvantage of this method is that it requires two-pieces of equipment rather than just one. The most effective method of manure collection is the elevating scraper. The scraper is pulled behind a tractor, and can be set to collect at a certain depth. This ensures that the interfacial layer will not be damaged and increases the quality of the harvested manure. Since the scraper needs to be pulled along, corners of a feedlot pen cannot be reached with the scraper, requiring the use of a box-blade or other equipment for collection in those areas. Due to its versatility, the wheel loader is the most common collection technique. Some feedlots are paved with fly ash. A wheel loader is used for collection from these pens since there is no interfacial layer to disturb.

Ash content of manure from these pens is lower than the ash content of the soil surfaced pens since no soil is collected during harvesting.

II.3 Fuel Properties

Due to the growing demand for renewable fuels, there are a wide variety of biomass fuels either being used in pilot scale plants or under laboratory investigation. The majority of these fuels fall into one of two categories, plant based biomass and animal waste biomass. The ultimate and proximate analyses as well as the higher heating value both on a dry and dry ash free basis of the plant based biomass fuels are given in table II.1 [2]. These fuels were analyzed as part of a study conducted for the National Renewable Energy Laboratory on the fouling characteristics of biomass fuels. Fouling is directly related to the ash content of the fuel and is a major concern for direct firing of biomass fuels.

Table II.1: Proximate and ultimate analysis of selected plant based biomass fuels [2]

Fuel:	Red Oak Sawdust	Mixed Paper	Sugar Cane Bagasse	Wheat Straw	Almond Shells
Proximate Analysis (% as recieved)					
Moisture	11.45	8.75	10.39	7.04	6.93
Fixed Carbon	11.92	6.78	10.70	16.47	19.28
Volatile Matter	76.35	76.87	76.72	69.97	70.73
Ash	0.28	7.60	2.19	6.52	3.06
Ultimate Analysis (% dry ash free)					
Carbon	50.12	52.35	49.86	48.31	50.98
Hydrogen	5.94	7.23	6.02	5.87	6.17
Oxygen (diff)	43.91	40.19	43.92	45.17	42.02
Nitrogen	0.03	0.15	0.16	0.47	0.79
Sulfur	0.01	0.08	0.04	0.17	0.04
Higher heating value (Dry)					
MJ/kg	19.42	19.05	18.53	16.68	18.85
Btu/lb	8348	8190	7967	7172	8102
Higher heating value (Dry Ash Free)					
MJ/kg	19.48	20.78	18.99	17.94	19.49
Btu/lb	8374	8934	8166	7714	8378

The as received proximate analysis shows a lot of similarity among the plant based biomass fuels; the major component being the volatile matter (70 – 77 % as received). The ultimate analysis again reveals the similarity between these fuels with carbon and oxygen contents varying by less than 5%. Both heating values given are also very similar for all but the wheat straw biomass.

Table II.2 gives the characteristics of different types of animal waste biomass fuels (AWBF). The selected fuels are all derived from animal manure, but other types of animal biomass could be included, i.e. animal carcasses (part of the future work at Texas A&M Universities Renewable Energy Lab). The four cattle biomass fuels on the left of the table are the test fuels for this research, while the data on the other fuels was gathered from literature. The diary biomass analysis is part of research gathered into the

feasibility of an advanced gasification system for a dairy farm in Upstate New York that could be used to eliminate excess dairy waste [3]. The data on sheep biomass was gathered by a research team at Pennsylvania State University. They are investigating the hardware, development, fuel evaluations, and emissions characteristics of biomass fuels and coal in industrial boilers [4]. The chicken litter biomass information was gathered at Texas A&M University as part of ongoing research by the Renewable Energy Lab into the disposal and utilization of excess animal waste [5].

Table II.2: Proximate and ultimate analysis of selected animal waste biomass fuels
Note: * - Results of TAMU REL

Fuel:	HAPC* Cattle Biomass	LAPC* Cattle Biomass	HARM* Cattle Biomass	LARM* Cattle Biomass	Dairy Cattle Biomass	Sheep Biomass	Chicken Litter Biomass
Proximate Analysis (% as recieved)							
Moisture	17.00	19.64	19.81	20.27	69.60	47.80	7.57
Fixed Carbon	3.36	11.54	6.02	12.16	N/A	7.30	8.41
Volatile Matter	25.79	52.33	27.08	51.47	N/A	34.00	40.22
Ash	53.85	16.50	47.10	16.10	8.96	10.90	43.80
Ultimate Analysis (% dry ash free)							
Carbon	51.19	52.91	52.56	53.99	44.65	51.33	45.14
Hydrogen	4.77	5.72	6.36	6.55	5.85	6.45	6.06
Oxygen (diff)	39.10	37.49	35.35	34.73	38.18	38.81	42.02
Nitrogen	3.87	3.08	4.70	3.90	2.05	2.65	5.41
Sulfur	1.08	0.79	1.03	0.84	0.31	0.76	1.37
Higher heating value (Dry)							
MJ/kg	6.27	16.51	7.86	16.81	18.22	16.04	9.98
Btu/lb	2697	7097	3380	7229	7834	6895	4291
Higher heating value (Dry Ash Free)							
MJ/kg	17.86	20.77	19.05	21.07	18.22	20.27	18.97
Btu/lb	7680	8930	8190	9058	7834	8715	8155

The as received analyses of the animal biomass fuels are much more varied than the plant biomass fuels, with moisture varying from 7-70%. The ash content of these fuels is also much higher than for the plant biomass fuels. However, the fuels are very similar when compared on a dry ash free (DAF) basis as in the ultimate analysis and the

DAF higher heating value. There is also a lot of similarity between the plant based biomass fuels (PBF) and the AWBF on a DAF basis. This is likely due to the strong relation between animal ration and animal waste [6], since cattle metabolic efficiency is approximately 20%.

Since much of the research on biomass fuels deals with co-combustion with coal, a table of various coals tested in literature is also presented here, table II.3. The table gives data from the two research coal being used at Texas A&M University, Texas lignite and Wyoming sub-bituminous, as well as four other coals. The data on the Cyprus bituminous and Alaskan lignite coals was gathered from the Korean Institute of Energy Research in which different candidate coal were compared to improve efficiency and reduce emissions through coal gasification [7]. The Greek lignite and Colombian coals were studied in conjunction with meat and bone meal (MBM) biomass in a study by the University of Crete, which looks into the combustion of MBM biomass as a means of waste disposal [8].

Table II.3: Proximate and ultimate analysis of selected coals
Note: * - Results of TAMU REL

Fuel:	Texas* Lignite Coal	Wyoming* Sub-bit. Coal	Cyprus Coal (USA)	Alaskan Coal	Greek Lignite	Colombian Coal
Proximate Analysis (% as recieved)						
Moisture	38.34	32.88	9.97	22.32	24.32	4.20
Fixed Carbon	25.41	32.99	44.22	29.19	30.59	53.00
Volatile Matter	24.79	28.49	42.25	36.75	31.30	36.60
Ash	11.46	5.64	3.56	11.75	13.79	6.20
Ultimate Analysis (% dry ash free)						
Carbon	74.06	75.68	66.36	48.24	61.25	83.40
Hydrogen	4.22	4.43	5.44	6.07	5.13	6.25
Oxygen (diff)	19.14	18.37	27.09	44.95	31.05	8.01
Nitrogen	1.35	1.07	0.95	0.62	1.83	1.56
Sulfur	1.22	0.45	0.16	0.12	0.73	0.78
Higher heating value (Dry)						
MJ/kg	23.17	27.11	25.33	22.60	20.16	28.23
Btu/lb	9962	11657	10890	9718	8666	12135
Higher heating value (Dry Ash Free)						
MJ/kg	28.46	29.60	26.37	26.63	24.65	30.18
Btu/lb	12236	12726	11338	11449	10598	12975

The proxiamte analyses conducted on these fuels shows how coals vary in different regions of the world. Even in the dry ash free ultimate anlayses, many differences can be noted, specifically carbon and oxygen contents. Overall, however, coals are much higher in heating value than biomass. For this reason, most research into biomass fuel technology is restricted to biomass being used as a suplementary fuel (i.e. co-firing or reburn).

II.4 Kinetics of Pyrolysis

Pyrolysis by definition is the decomposition or transformation of a compound caused by heat. There are two major steps to the pyrolysis of most fuels. First, any moisture in the fuel will evaporate, and second, volatile compounds, CH_4, CO, CO_2, etc.,

will be driven off. Kinetics parameters such as activation energy and pre-exponential factor can be determined from measured parameters such as weight change, time, and temperature recorded during pyrolysis. Measurements are made using a thermogravimetric analyzer (TGA) for relatively slow heating rates, i.e. < 100 K/min. The basic first order kinetics model of pyrolysis is given below:

$$-\frac{dm_v}{m_v} = k_0 \cdot \exp\left(-\frac{E}{\overline{R} \cdot T}\right) dt \qquad \text{(II.1)}$$

Where m_v is the mass of the volatiles remaining in the sample (DAF), k_o is the frequency factor or pre-exponential factor, E is the activation energy, $\overline{R}$ is the universal gas constant, T is the temperature, and t is time. The preceding reaction is known as the single reaction model [9]. Details to the solution of this equation are given in chapter V. It has been shown that the single reaction model does not adequately represent the kinetics of pyrolysis for coal or biomass fuels since the fuel consists of several decomposable polymers which break down into monomers and other compounds. Consequently, a new model was needed.

Dutta et al. (1977) [10] conducted pyrolysis of Pittsburgh HVab coal and Illinois no 6 coal using a Fisher TGA. The coal pyrolysis is complete around 350°C to 400°C and the volatile yields correspond to the proximate yields. Anthony *et al*. (1974) [11] conducted experiments using 5-10 mg monolayer samples of lignite and bituminous coal in the range of 400°C to 1000°C and found that the weight loss depends on the final temperature, but not on heating rate for heating rates less than 10,000 K/s. They

formulated a distributed activation energy model, where a Gaussian distribution represented the activation energy, equation (II.2).

$$-\frac{dm_{v_i}}{\left(m_{v,i}\right)} = k_{0,i} \cdot \exp\left(-E_i / \overline{RT}\right) \cdot dt \qquad \text{(II.2)}$$

The subscript *i* in equation (II.2) implies that the activation energy does not have a single value but rather has multiple values. Anthony *et al*. further theorized that the distribution of activation energies could be fit to a Gaussian distribution *f(E)* with mean activation energy E_m and standard deviation σ. Using the model they were able to determine the kinetics values for several species of coal with reasonably accurate results; however, the solution to equation (II.2) requires a complex double integration as seen in equation (II.3). The full derivation of equation (II.3) along with *f(E)* is given in chapter V. Anthony *et al*. found the mean activation energies for two coals, Montana Lignite and Pittsburgh Seam Bituminous, to be 236 kJ/mol and 212 kJ/mol with standard deviations 46 kJ/mol and 29 kJ/mol, respectively.

$$\left(\frac{m_v}{m_{v,0}}\right) = \int_{E_m-3\sigma}^{E_m+3\sigma} \exp\left\{-\int_{T_0}^{T} \frac{k_0}{\beta} \cdot \exp\left(-\frac{E_i}{\overline{RT}}\right) \cdot dT\right\} f(E)\,dE \qquad \text{(II.3)}$$

Later, Raman *et al*. (1981) applied the distributed activation energy model to feedlot biomass to determine the effects TGA parameters had on the activation energy and standard deviation. The manure used in this study was collected from paved feedlots at Kansas State University's Beef Research Center [12]. They concluded that thermogravimetric parameters such as heating rate, size fraction, and purge gas flow rate had no effect on E_m, but σ was affected by the heating rate and purge gas flow rate.

Their results indicated a mean activation energy of 176 kJ/mol with standard deviation 27 kJ/mol.

The review by Annamalai et al (1995) [13] revealed that the experiments involving variations of sample masses resulted in different volatile yields: ASTM: 1000 mg, TGA: 15-30 mg, Crucible Experiments: 10-20 mg, Heated Grids: 5-10 mg, Flash heating <10 mg. Thus, apart from kinetic and thermo-physical parameters, the size of sample or group effects will also affect the volatile yields. While extensive data is available for coal, only limited studies have been conducted on pyrolysis of animal waste.

More recent work in this area has been to make improvements to the distributed activation energy model to make the equation easier to solve and/or to better approximate results. One alteration of the DAEM was proposed by Donskoi and McElwain (1998) [14]; they related the activation energy and pre-exponential factor directly to the heating rate. Their model was applicable to models with a large number of heating rates, and it significantly cut down on the time for calculation without an appreciable change in the accuracy of the calculation. Another approach taken by Donskoi and McElwain (2000)[15] was to use a modified Gauss-Hermite Quadrature method to evaluate the double integration in equation (3) in order to lower the error of integration as well as reduce the computation time. Other attempts to reduce computation time were proposed by Please et al. (2003) [16] in which asymptotic expansions were used to rapidly arrive at a solution. Two assumptions of the distributed activation energy model are that the distribution, *f(E)*, is Gaussian and the k_o term in

equation (II.3) is constant ($1.67*10^{13}$ 1/s). The assumption for a constant k_o is valid for small values of σ, but not for wider activation energy ranges. The fuels being tested at Texas A&M University's Renewable Energy Lab were tested using distributed activation energy model with a constant value for k_o to simplify the calculation. Jinno et al (2004) [17] studied the decomposition behavior of surrogate solid wastes (cellulose, polyethylene, polypropylene, polystyrene and polyvinyl chloride) in inert (N2) and oxidizing (air) gases. They extracted the pyrolysis kinetics using single global first order reaction model and determined half decomposition (50 % mass loss) temperatures as 344-395 C for cellulose (lower heating rate (HR): 5 C/min, higher HR: 50 C/min), 430-490 C for polypropylene, 388-457 C for polystyrene, and 290-340 C for polyvinyl chloride. The corresponding values in air were consistently lower with values of 325, 298, 281, 362 and 279 C respectively at HR= 5 C/min. It should be noted that these samples were homogeneous in makeup, and a single reaction model could be used. For fuels with a wide variety of components, the parallel reaction model produces results that are more accurate.

II.5 Ignition

When TGA is performed in N_2, only pyrolysis occurs. If the experiment is repeated in air, oxidation can also occur simultaneously. The experiments in air can also be used to define the onset of ignition of fuel samples in TGA. Tognotti et al (1985) [18] used TGA techniques to determine the ignition temperature of coal particles and found that the ignition temperature of sample is lower than the single particle ignition temperature.

II.6 Scope of Work

The techniques described in the literature for fuel characterization are applied to coal, four types feedlot biomass, and blends of coal with biomass. This includes fuel property evaluation, pyrolysis modeling, and ignition modeling. The fuel property evaluation includes comparisons of ultimate and proximate analyses as well as ash characterization comparisons. The pyrolysis modeling is conducted using both a single reaction model and the distributed activation energy model, and pyrolysis kinetics are determined. In addition, ignition studies are performed to determine fuel ignition temperatures.

CHAPTER III

OBJECTIVES / TASKS

The overall objective of this research is to evaluate the pyrolysis and ignition behavior of four types of feedlot biomass (FB), Texas lignite coal (TXL), and blends of biomass with TXL. The fuels being considered are High Ash Raw Manure (HARM), Low Ash Raw Manure (LARM), High Ash Partially Composted Manure (HAPC), Low Ash Partially Composted Manure (LAPC), Texas Lignite Coal (TXL), and Wyoming Sub-bituminous Coal (WSB). Low ash samples of each FB will be collected from feedlot pens with a fly ash surface, while high ash samples will be collected from soil surfaced enclosures. The FB samples are representative of the types of fuels which may be fired in a utility boiler either as reburn fuel or co-firing fuel. In order to achieve the overall objective, the following tasks were performed:

A. Obtain fuel samples and determine fuel characteristics

- **i.** Gather fuel samples from members of our research team in the Amarillo, TX area. Once prepared, send samples to the renewable energy lab (REL) in College Station, TX.
- **ii.** Obtain fuel characteristics using a commercial testing company

B. Write specification for and obtain thermogravimetric analyzer TGA

- **i.** This task requires an investigation into commercially available thermogravimetric analyzers and a review of the needs of the REL research group. Once completed, purchase the TGA through bid process.

C. Classify fuel samples by particle size

i. Sieve prepared fuel samples, and classify according to particle size using available REL equipment.

ii. Selected particle sizes: As Received, 60 micron and 22.5 micron based on sieve sizes available.

D. Determine blend ratios and blend fuels for testing

i. Mix biomass fuels with coal in varying amounts to determine what effect this has on the kinetics parameters under investigation. Determine specific blend ratios through coordination with other group members to ensure consistency in results. Blends are on a mass basis.

ii. Test the following blend ratios (FB/TXL): 100/0, 50/50, 30/70, 10/90, and 0/100

E. Test fuel sample in TGA in both N2 and air environments

i. Include TGA software package and necessary training for operation of the equipment with the TGA specification. After training is completed testing begins.

F. Create methods for fuel characteristics calculations. (From available literature necessary formulas and theory have been gathered to make calculations.)

i. Create an Excel based spreadsheet to calculate activation energy using the single reaction model described in the literature review solving the following equations for activation energy E:

$$-\ln\left(\frac{m_v}{m_{vo}}\right)=\left(\frac{B}{\beta}\right)\cdot\left(\frac{E}{\overline{R}}\right)\cdot\left(\frac{\mathrm{E}_2(X)}{X}-\frac{\mathrm{E}_2(X_o)}{X_o}\right)$$

ii. Create an Excel based spreadsheet to determine the ignition temperature using the relationship (ignition temperature is the point where this statement is true and remains true as temperature increases):

$$\frac{(m\%)_{N2}-(m\%)_{air}}{\left[\frac{(m\%)_{N2}+(m\%)_{air}}{2}\right]}>5\%$$

iii. Create a MatLAB based program to calculate the activation energy using the distributed activation energy model to solve the following equation and obtain a value for activation energy E (this equation must be solved numerically, hence the necessity of a MatLAB based program):

$$\frac{m_v}{m_{v,0}}(T) = \frac{1}{\sigma\sqrt{2\pi}} \cdot \int_0^{\infty} \exp\left\{ -\frac{k_0}{\beta} \cdot \left[T \cdot \mathrm{E}_2\left(\frac{E}{R \cdot T}\right) - T_0 \cdot \mathrm{E}_2\left(\frac{E}{R \cdot T_0}\right) \right] - \frac{(E - E_m)^2}{2 \cdot \sigma^2} \right\} dE$$

G. Use the created calculations tools to determine characteristics described in the objectives.

H. Report the results for kinetics of pyrolysis and comparative ignition behavior of biomass fuels, coal, and blends.

CHAPTER IV

EXPERIMENTAL SETUP AND TEST PROCEDURE

IV.1 Chapter Overview

The following chapter gives specific details on the types how the fuel testing was carried out. First, the types of fuels used for this study are defined, and preparation of the fuel samples is described. Next, the setup of the Thermogravimetric Analyzer is reviewed in detail for future work with the instrument. Lastly, the test procedure used is given along with appropriate explanation of why different aspects of the procedure are necessary.

IV.2 Sample Preparation

The four types of feedlot biomass being tested (LAPC, HAPC, LARM, HARM) were sieved to separate the sample into particle size groups. Three particle sizes were selected to show the effect particle size has on reaction kinetics: As Received (AR), between 75 and 45 μm (average 60 μm) and below 45 μm (22.5 μm). While the actual distribution of particle sizes between sieves is unknown, the particle classifications are identified by the mean values. Once separated, each sample was mixed with Texas Lignite Coal of like particle size in the following concentrations: 90:10, 70:30, and 50:50 (TXL %: FB %). In addition, tests were conducted on pure biomass samples as well as the Texas Lignite Coal in each size classification for a total of 51 samples.

IV.3 Thermogravimetric Analyzer Setup

All thermal decomposition tests were performed using a TA Instruments Q600 thermal analyzer. The analyzer is capable of Thermogravimetric Analysis (TGA), ± 1% accuracy, as well as Differential Scanning Calorimetry (DSC) measurements.

Setup of the thermal analyzer was straightforward. A 120 V, 60 hz power connection was required as well as an Ethernet connection to a computer. Other required connections were for carrier gases and purge gas. The carrier gases used were N_2 for pure pyrolysis and air for oxidation and kinetics studies, regulated below 20 psi as required by the manufacturer. The purge gas used was air, which is used to cool the furnace after testing. A schematic of the TGA is shown in figure IV.1.

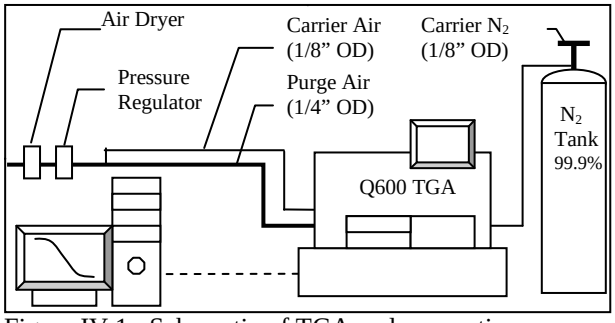

Figure IV.1: Schematic of TGA and connections

Measurements were made using TA Instruments software, and equipment calibration was performed by TA instruments personnel during the software installation prior to the beginning of testing. The Q600 has a wide range of test parameters that can be tuned for a particular test or adjusted as independent variables during testing. The principle of operation for the Q600 can be found in the appendix A. For the tests being conducted, temperature, time, particle size, and sample composition are considered independent

variables, while weight and heat flow are dependent variables. Other possible variables include initial temperature, final temperature, heating rate, carrier gas flow rate, and sample size, which were held fixed during testing, see table IV.1 These parameters affect the shape of the weight vs. temperature/time trace (thermo-gram) obtained from the TGA; they were chosen to minimize error between actual and calculated thermo-grams.

Table IV.1: TGA test parameters

Test Parameters				
Initial Temp	~300	(K)	~75	(℉)
Final Temp	1373	(K)	2012	(℉)
Heating Rate	40	(K/min)	72	(℉/min)
Gas Flow Rate	50	(ml/min)	3.05	(in^3/min)
Sample Size	~10	(mg)	~3.5E-4	(oz)

IV.4 Test Procedure

Software

The software package included with the thermal analyzer was a windows based program that allowed for easy changes to the test procedure. A typical test procedure was as follows:

1. Select Gas (1 for N_2, 2 for Air)
2. Set Gas Flow Rate to 200 ml/min (0 – 1050 ml/min)
3. Heat at 40 K/min (0 – 100 K/min)
4. Hold at 423 K (150 °C) for 5 min
5. Set Gas Flow Rate to 50 ml/min
6. Heat at 40 K/min to 1373 K (1100 °C)

The initial gas flow rate was set to 200 ml/min for 5 minutes at 423 K to fully purge the furnace of gaseous impurities before testing and dry the sample, ensuring that any changes in the temperature/weight trend are due to volatile losses or ignition depending

on the carrier gas. The heating rate is set to 40 K/min to maximize the slope of the temperature/weight trend for calculations without causing excess equipment wear, the higher this value, the greater the slope.

Hardware

The TGA had to be preheated if it had a been idle; this was done by heating the furnace to 1273 K and cooling without a sample. The sample cups were alumina and had a 90 μL capacity. To begin testing, the furnace was opened, and the sample cups checked for any residual material and cleaned if necessary. The furnace was then closed to tare the balances. The Q600 had a dual beam balance capable of measuring up to 350 mg each. After tarring, the furnace was opened and the test cup was removed, noting the orientation before removal. The test cup was nearest the front of the machine; the other cup was a reference cup used for heat flow calculations (DSC), see Figure IV.2.

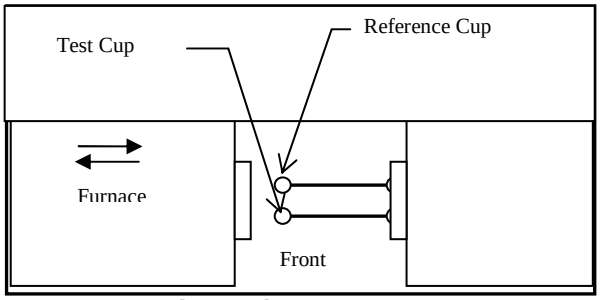

Figure IV.2: Balance schematic

Once removed, 10 mg of the fuel sample was added to the cup, ensuring that no excess material was on the top or exterior of the sample cup. These could damage the platinum thermocouples embedded in the balance at the bottom surface of the cups. The sample cup was replaced in the same orientation, and the furnace closed to begin testing.

CHAPTER V

THEORY

V.1 Chapter Overview

Chapter V presents the methods used to interpret and analyze the characteristics of the fuels including fuel properties, kinetics of pyrolysis and ignition temperature. Section two gives the calculations performed from the ultimate and proximate analyses. The third section explains the single reaction model for pyrolysis and its limitations when applied to coal / biomass pyrolysis, while the fourth section gives an in depth description of the distributed activation energy model for pyrolysis and the method of solution. The final section gives a simplified methodology on determining the ignition temperature of coal, biomass, and biomass blends.

V.2 Fuel Properties

Ultimate and proximate analyses were performed on each of the five test fuels; several fuel properties were calculated based on these results including the Sauter Mean Diameter (SMD), volatile matter higher heating value (HHV_{VM}), mass based stoichiometric air/fuel ratio (A:F ratio), and adiabatic flame temperature (AFT).

The SMD calculations were based on the sieved sample classifications. Sieve sizes in microns were as follows: 2000, 1191, 840, 300, 150, 75, and 45 (sieve numbers: 10, 16, 20, 50, 100, 200, and 325 respectively). A total of 300 grams of each fuel was sieved, and the material collected in each sieve was then weighed. From the sieved samples the SMDs were calculated using equation (V.1).

$$SMD = \frac{\sum N_i \cdot d_i^{\,3}}{\sum N_i \cdot d_i^{\,2}} = \frac{1}{\sum Y_i / d_i} \qquad \text{(V.1)}$$

Where N_i is the number of particles of diameter d_i, Y_i is the mass fraction of the particles in each sieve classification, and d_i is the average of the two sieve sizes for each range, i.e. (300 – 150 → d_i=225).

Higher heating values for the volatile matter in the fuels were also calculated using equation (V.2).

$$HHV_{VM} \cong \frac{\left(HHV - FC\% \cdot HHV_{FC}\right)}{VM\%} \qquad \text{(V.2)}$$

Where HHV is the as received higher heating value, FC% is the amount of fixed carbon in the fuel, HHV_{FC} is the higher heating value of the fixed carbon (enthalpy of formation / molecular weight of carbon), and VM% is the amount of volatile matter in the fuel. Equation V.2 assumes that the heat of pyrolysis is negligible [9].

The mass based stoichiometric air/fuel ratio (A:F ratio) for each of the fuels was calculated based on atom balancing from the empirical formulas and empirical molecular weights. Similarly, the adiabatic flame temperature for each of the fuels was determined from empirical values.

V.3 Single Reaction Model

Using the previously described testing procedure, thermo-grams were generated for the fuel samples using N_2 as the carrier gas; a sample trace is shown in figure V.1. Region A-B represents the mass loss due to moisture evaporation, region B-C is heating to pyrolysis temperature, region C-D represents the primary volatile loss, and region D-E represents the remaining volatile loss. The thermo-grams are then analyzed to determine

the activation energy based on the primary volatile loss region C-D. Volatiles include CO_2, CH_4, H_2, etc. and are released at different rates. Activation energies can also be calculated for the secondary loss region D-E, but these analyses are left for future researchers. Activation energy is the energy required for a chemical reaction to occur, and is related to the collision energy and frequency between molecules.

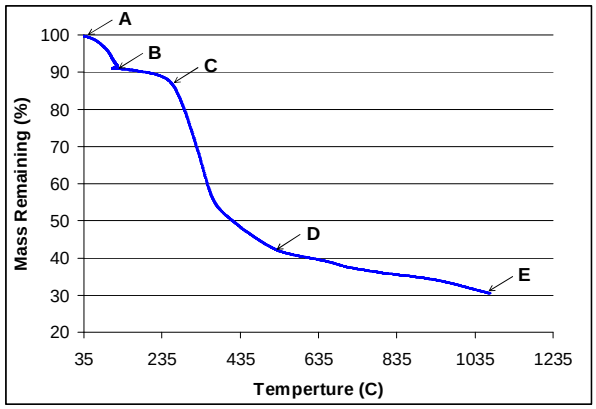

Figure V.1: Sample thermo-gram

The volatile mass loss, region C-D, was first modeled using a single reaction model given in equation (V.3).

$$-\frac{dm_v}{dt} = k(T) \cdot m_v \qquad \text{(V.3)}$$

Where m_v is the mass of volatiles remaining in the solid at time t and $k(T)$ is given by the Arrhenius expression [9]:

$$k(T) = k_0 \cdot \exp(-E/\overline{R}\,T) \qquad \text{(V.4)}$$

Where T is temperature, k_o is frequency factor, E is activation energy, and $\overline{R}$ is the gas constant. Inserting equation (V.4) into equation (V.3) and rearranging yields equation (V.5).

$$-\frac{dm_v}{m_v} = k_0 \cdot \exp\left(-E/\overline{R}T\right) \cdot dt \tag{V.5}$$

Under the thermogravimetric analysis dT/dt was held constant at 40 K/min, so equation (V.5) can be rewritten in terms of a temperature differential.

$$-\frac{dm_v}{m_v} = \frac{k_0}{\beta} \cdot \exp\left(-E/\overline{R}T\right) \cdot dT \tag{V.6}$$

Thus, after integration we obtain equation (V.7).

$$-\ln\left(\frac{m_v}{m_{vo}}\right) = \left(\frac{k_0}{\beta}\right) \cdot \int_{T_o}^{T} \exp\left(\frac{E}{\overline{R} \cdot T}\right) \cdot dT \tag{V.7}$$

Where m_{vo} is the initial mass of volatiles at T_o and $\beta = dT/dt$. Equation (V.7) was used to find values for E and k_o in two different ways, a slope approximation and second by a more rigorous exponential integral solution. Note that $m_v = m - m_{ash} - m_{H_2O}$, and $m_{vo} = m_o - m_{ash} - m_{H_2O}$. Thus,

$$\ln\left(\frac{m_v}{m_{vo}}\right) = \ln\left(\frac{m - m_{ash} - m_{H_2O}}{m_o - m_{ash} - m_{H_2O}}\right) = \ln\left(\frac{m_{DAF}/m_o}{VM_{o,DAF}}\right) \tag{V.8}$$

Method A: Slope Approximation

An approximation for the right side of equation (V.7) is given in equation (V.9); this solution is only valid for $20 < E/\overline{R}T < 60$ [9].

$$-\ln\left(\frac{m_v}{m_{vo}}\right) \cong 0.00482 \cdot \frac{E \cdot k_0}{\overline{R} \cdot \beta} \cdot \exp\left(-1.052 \cdot \left(\frac{E}{\overline{R} \cdot T}\right)\right) \tag{V.9}$$

Equation (V.9) can be rewritten as

$$\ln\left[-\ln\left(\frac{m_v}{m_{vo}}\right)\right] \cong \ln\left[\left(\frac{k_0}{\beta}\right) \cdot \left(0.00482 \cdot \frac{E}{\overline{R}}\right)\right] + \left(-1.052 \cdot \left(\frac{E}{\overline{R}}\right) \cdot \left(\frac{1}{T}\right)\right) \tag{V.10}$$

A value for activation energy was found by plotting $\ln[-\ln(m_v/m_{vo})]$ vs. $1/T$ and determining the slope, see Figure V.2. The slope of the resulting line was $-1.052 \cdot (E/\overline{R})$. Then the validity of the approximation was verified by determining if $20 < E/\overline{R}T < 60$ is true. Once the activation energy was obtained a value for the frequency factor was directly calculated from equation (V.9).

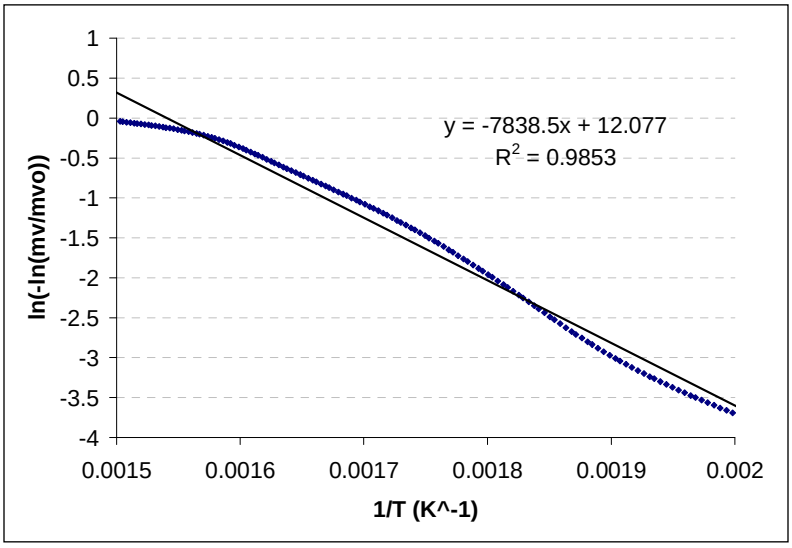

Figure V.2: Slope method evaluation curve

Method B: Rigorous Solution

Due to the limited range of equation (V.9), an exponential integration method [9] was also used, see equation (V.11a,b).

$$\int_{T_0}^{T} \exp\left(-E/\overline{R}T\right)\cdot dT = \left(\frac{E}{\overline{R}}\right)\cdot\left\{\frac{\mathrm{E}_2(X)}{X} - \frac{\mathrm{E}_2(X_0)}{X_0}\right\} \tag{V.11a}$$

Where $X = E/\overline{R}T$, $X_0 = E/\overline{R}T_0$, and the functions E_n are:

$$\mathrm{E}_2(X) = \exp(-X) - X\cdot\mathrm{E}_1(X)$$
$$\mathrm{E}_1(X)\cdot X\cdot\exp(X) = \frac{X^2 + 2.334733\,X + 0.250621}{X^2 + 3.330657\cdot X + 1.681534} \tag{V.11b}$$

Equation (V.8) can now be rewritten in terms of the exponential integrals described in equations (V.11a, b):

$$-\ln\left(\frac{m_v}{m_{vo}}\right) = \left(\frac{B}{\beta}\right)\cdot\left(\frac{E}{\overline{R}}\right)\cdot\left(\frac{\mathrm{E}_2(X)}{X} - \frac{\mathrm{E}_2(X_o)}{X_o}\right) \tag{V.12}$$

Values for activation energy E and frequency factor k_o were found iteratively. First, values were assumed for both. These values were used to obtain a calculated value for (m_v/m_{vo}) for a range of temperatures representing the primary volatile loss, see figure V.3. The values for activation energy and frequency factor were then iterated to minimize the squared error between the calculated and actual values of (m_v/m_{vo}).

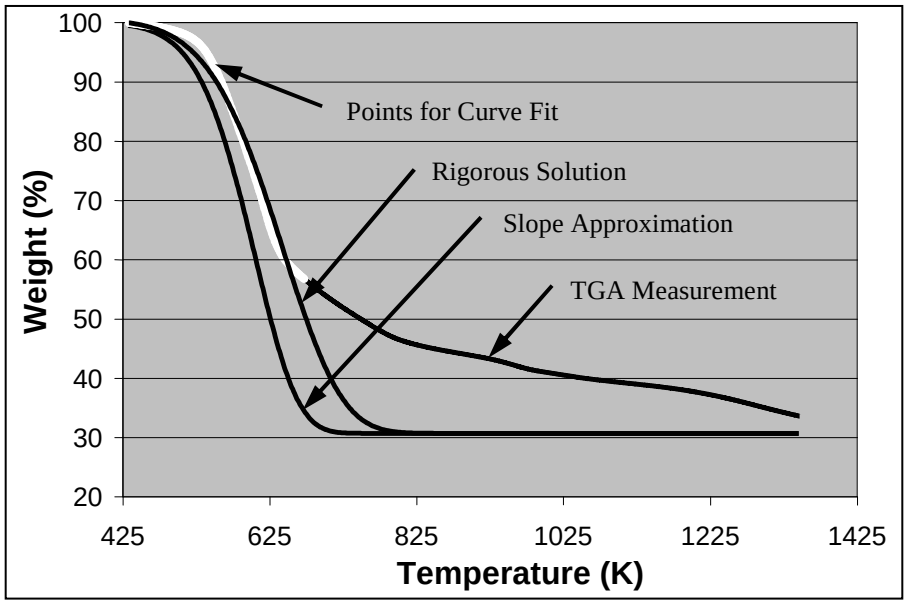

Figure V.3: Mass remaining vs. temperature trace with the single reaction model activation energy solution methods A & B

Method C: Maximum Volatile Release Rate

As temperature in the sample increases the volatile release rate also increases due to the increased temperature. As the amount of volatiles in the fuel decreases, the volatile release rate slows, and eventually begins to decrease even though temperature is still increasing, creating a maximum volatile release rate (MVRR), $(dm_v/dt)_{max}$, at $T = T_{max}$. Equation (V.6) is rewritten with two key differences, the differentials are grouped on the left with everything else on the right and the term n_v is introduced indicating the order of the reaction, equation (V.13)

$$-\frac{dm_v}{dT} = \frac{k_0}{\beta} \cdot m_v^{\,n_v} \cdot \exp\left(-E/\bar{R}T\right) \tag{V.13}$$

Equation (V.13) is differentiated with respect to T to obtain equation (V.14)

$$-\frac{d^2 m_v}{dT^2} = \frac{k_0}{\beta} \cdot \left[n_v \cdot m_v^{(n_v - 1)} \cdot \frac{dm_v}{dT} \cdot \exp\left(-\frac{E}{\overline{R} \cdot T} \right) + m_v^{n_v} \cdot \left(\frac{E}{\overline{R} \cdot T^2} \right) \cdot \exp\left(-\frac{E}{\overline{R} \cdot T} \right) \right] \qquad \text{(V.14)}$$

The maximum volatile release rate occurs when d^2m_v/dT^2 is zero; so after setting equation (V.14) equal to zero and rearranging one obtains equation (V.15).

$$-\frac{dm_v}{dT} = \frac{m_v^{n_v}}{n_v \cdot m_v^{(n_v - 1)}} \cdot \left(\frac{E}{\overline{R} \cdot T^2} \right) \qquad \text{(V.15)}$$

With the assumption of a first order reaction with $n_v=1$, the activation energy can now be found for $(dm_v/dt)_{max}$ at $T = T_{max}$, equation (V.16).

$$-\left(\frac{dm_v}{dT} \right)_{\max} = m_{v,\max} \cdot \left(\frac{E}{\overline{R} \cdot T_{\max}^{\ 2}} \right) \qquad \text{(V.16)}$$

The frequency factor k_o is calculated by equating equations (V.13) at $T=T_{max}$ and (V.16).

$$\frac{k_0}{\beta} \cdot = \cdot \left(\frac{E}{\overline{R} \cdot T_{\max}^{\ 2}} \right) \exp\left(E / \overline{R} T_{\max} \right) \qquad \text{(V.17)}$$

V.4 Distributed Activation Energy Model

It has been shown that the single reaction model does not adequately describe the kinetic behavior of a complex composition like coal; typically they consist of multiple chemical groups [11]. For this reason, the kinetics of pyrolysis for coal and biomass fuels were also calculated using the distributed activation energy model. In this model, it is assumed that the pyrolysis process consists of a series of reactions proceeding in parallel, Anthony et al. (1974). First order devolatilization for the i-th component of the reaction is given by equation (V.18):

$$-\frac{dm_{v,i}}{dt} = k_i \cdot \left(m_{v,i} \right) \qquad \text{(V.18)}$$

Equation (V.18) is evaluated in the same manor as equation (V.3 – V.7) to obtain:

$$\left(\frac{m_{v,i}}{m_{v,0,i}}\right) = \exp\left\{-\int_{T_0}^{T} \frac{k_{0,i}}{\beta} \cdot \exp\left(-\frac{E_i}{RT}\right) \cdot dT\right\} \tag{V.19}$$

If the range of values of activation energy *E* is assumed to be continuous and represented by the probability distribution function *f(x)* such that:

$$\int_{-\infty}^{\infty} f(x)dx = 1 \tag{V.20}$$

Then integration of equation (V.19) over all values of *E* gives the mass fraction of volatiles:

$$\left(\frac{m_v}{m_{v,0}}\right) = \int_{-\infty}^{\infty} \exp\left\{-\int_{T_0}^{T} \frac{k_0}{\beta} \cdot \exp\left(-\frac{E_i}{RT}\right) \cdot dT\right\} f(E)dE \tag{V.21}$$

Assuming the distribution function *f(E)* is Gaussian then *f(E)* can be written as:

$$f(E) = \frac{1}{\sigma \cdot \sqrt{2\pi}} \exp\left(-\frac{(E - E_m)^2}{2 \cdot \sigma^2}\right) \tag{V.22}$$

Where E_m is the mean activation energy, and σ is the standard deviation of activation energy, see figure V.4.

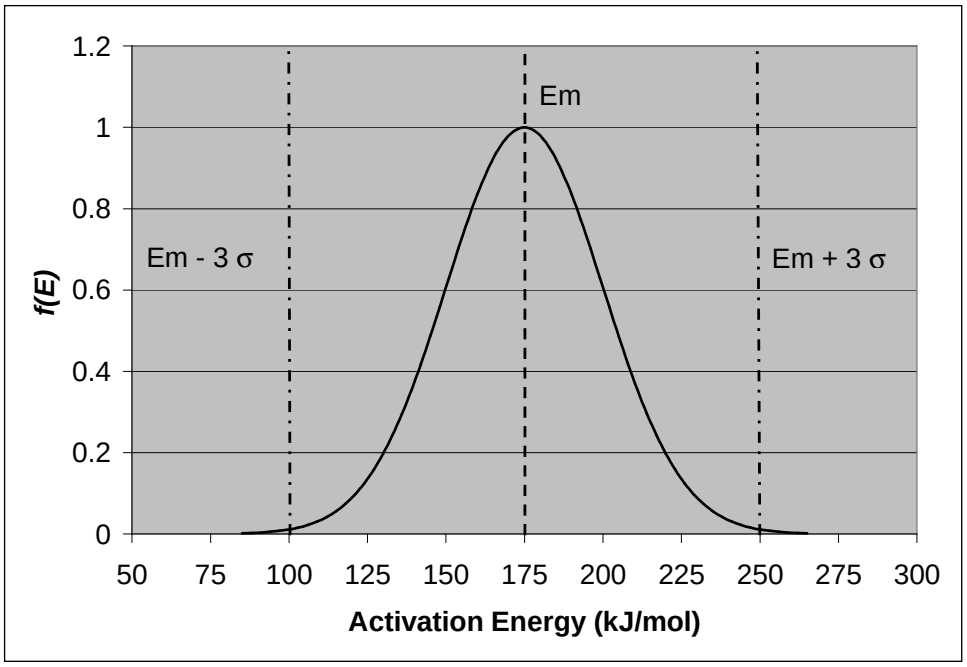

Figure V.4: Gaussian distribution function

Since *f(E)* is approximately zero at $E_m \pm 3\sigma$, the limits of integration are changed from $\pm\infty$ to $E_m \pm 3\sigma$ [11]. Taking this into consideration as well as equation (V.22), equation (V.21) becomes:

$$\left(\frac{m_v}{m_{v,0}}\right) = \frac{1}{\sigma \cdot \sqrt{2\pi}} \cdot \int_{E_m-3\sigma}^{E_m+3\sigma} \exp\left\{-\int_{T_0}^{T} \frac{k_0}{\beta} \cdot \exp\left(-E/\overline{RT}\right) \cdot dT\right\} \cdot \exp\left\{-\frac{(E-E_m)^2}{2 \cdot \sigma^2}\right\} dE \qquad \text{(V.23)}$$

The inner integral of equation (V.23) can be written in terms of the exponential integrals defined earlier in equation (V.11a):

$$\int_{T_0}^{T} \exp\left(-E/\overline{RT}\right) \cdot dT = \left(\frac{E}{\overline{R}}\right) \cdot \left\{\frac{\mathrm{E}_2(X)}{X} - \frac{\mathrm{E}_2(X_0)}{X_0}\right\} \qquad \text{(V.11a)}$$

Substituting equation (V.11a) into equation (V.23) and rearranging, the volatile mass fraction is now a function of temperature:

$$\frac{m_v}{m_{v,0}}(T)=\frac{1}{\sigma\sqrt{2\pi}}\cdot\int_{E_m-3\sigma}^{E_m+3\sigma}\exp\left\{-\frac{k_0}{\beta}\cdot\left(\frac{E}{\overline{R}}\right)\cdot\left[\frac{\mathrm{E}_2\left(E/\overline{R}T\right)}{E/\overline{R}T}-\frac{\mathrm{E}_2\left(E/\overline{R}T_0\right)}{E/\overline{R}T_0}\right]-\frac{(E-E_m)^2}{2\cdot\sigma^2}\right\}dE \tag{V.24}$$

With further simplification, equation (V.24) becomes:

$$\frac{m_v}{m_{v,0}}(T)=\frac{1}{\sigma\sqrt{2\pi}}\cdot\int_{E_m-3\sigma}^{E_m+3\sigma}\exp\left\{-\frac{k_0}{\beta}\cdot\left[T\cdot\mathrm{E}_2\left(\frac{E}{\overline{R}\cdot T}\right)-T_0\cdot\mathrm{E}_2\left(\frac{E}{\overline{R}\cdot T_0}\right)\right]-\frac{(E-E_m)^2}{2\cdot\sigma^2}\right\}dE \tag{V.25}$$

Equation (V.25) was solved numerically for values of temperature to generate a trace of volatile mass fraction vs. temperature for comparison to measured data. The simplest solution is an application of the trapezoid rule, which requires computation of values for the integrand of equation (V.25), henceforth referred to as *P(E, T).*

$$P(E,T)=\exp\left\{-\frac{k_0}{\beta}\cdot\left\{T\cdot\mathrm{E}_2\left(\frac{E}{\overline{R}\cdot T}\right)-T_0\cdot\mathrm{E}_2\left(\frac{E}{\overline{R}\cdot T_0}\right)\right\}-\frac{(E-E_m)^2}{2\cdot\sigma^2}\right\} \tag{V.26}$$

The function *P* will be represented as a matrix for values of E between E_m-3σ and E_m+3σ and values of T between T_0 and T_n (beginning and end of pyrolysis respectively).

$$P(E,T)=\begin{vmatrix} P(E_m-3\sigma,T_0) & \cdots & \cdots & \cdots & P(E_m-3\sigma,T_n)\\ \vdots & & & & \vdots\\ \vdots & & & & \vdots\\ \vdots & & & & \vdots\\ P(E_m+3\sigma,T_0) & \cdots & \cdots & \cdots & P(E_m+3\sigma,T_n)\end{vmatrix} \tag{V.27}$$

A value of volatile mass fraction (*mv/mv$_0$*) can now be calculated for each column of *G*. The values for E_m and σ were optimized by minimizing the squared error between the theoretical volatile mass fraction from equation (V.25) and measured volatile mass

fraction. The value for k_0 was assumed to be $1.67*10^{13}$ (1/sec) from transition state theory, Anthony et al. (1974). Figure V.5 shows a sample plot of theoretical and measured mass loss traces.

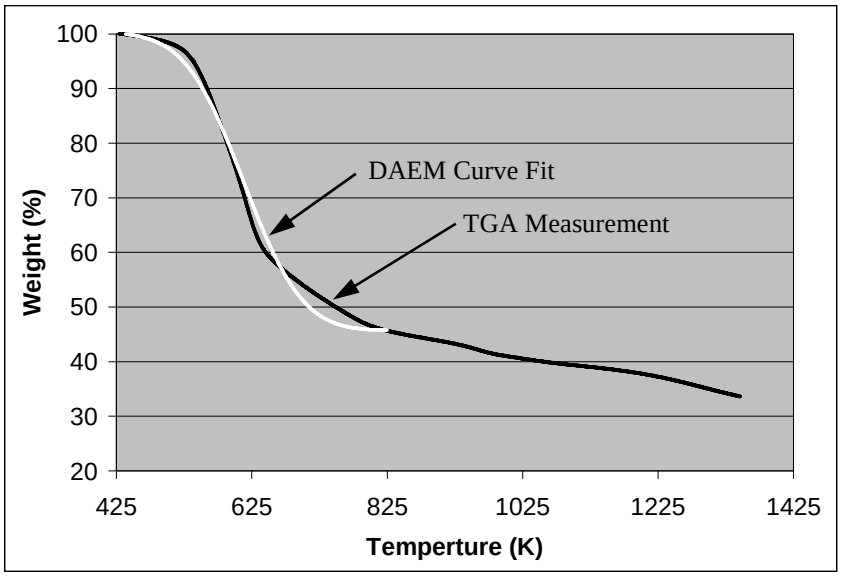

Figure V.5: Mass remaining vs. temperature trace with the distributed activation energy model solution method

V.5 Ignition

Ignition temperatures for the fuel samples were found graphically by comparing the air and N2 thermo-grams for a particular fuel. The ignition temperature is defined as the point at which the difference between the moisture normalized traces begin to deviate by more than 5% of the average value at that point and continues to deviate thereafter, see figure V.6.

$$\frac{(m\%)_{N2} - (m\%)_{air}}{\left[\frac{(m\%)_{N2} + (m\%)_{air}}{2}\right]} > 5\% \qquad \text{(V.28)}$$

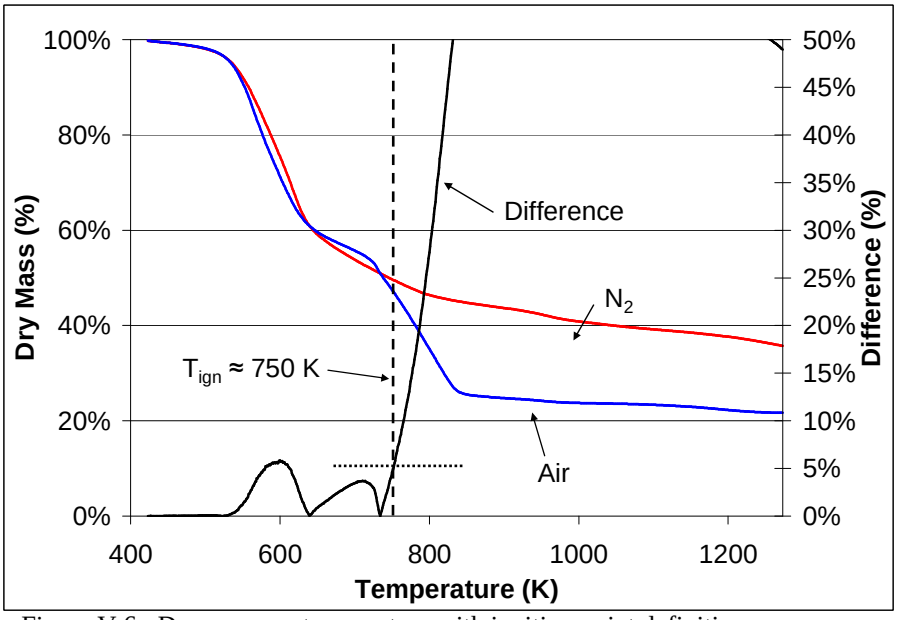

Figure V.6: Dry mass vs. temperature with ignition point definition

CHAPTER VI

RESULTS AND DISCUSSION

VI.1 Chapter Overview

Chapter VI focuses on the results obtained during testing in similar sections as chapter V. Section two presents the ultimate and proximate analyses as well as a few calculations based on the ultimate and proximate analyses. The third section focuses on single reaction model kinetics of pyrolysis, and section four gives kinetics values based on the distributed activation energy model. The last section gives the ignition temperatures for the various fuels and blends.

VI.2 Fuel Properties

A sample of each of the test fuels was sent to Hazen Research, Inc. in Golden, CO for ultimate and proximate analyses. The values presented here are an average of three tests performed on each of the samples. Two of the biomass fuels were chosen to show the differences between the three samples of each fuel tested. Low ash partially composted biomass is plotted in figureVI.1a, and high ash raw manure is plotted in figure VI.1b. For the LAPC sample, the largest differences are the moisture content, while for the HARM sample variations can be seen in the carbon, oxygen, ash, and moisture contents. However, these variations are all less than 10% of the average value.

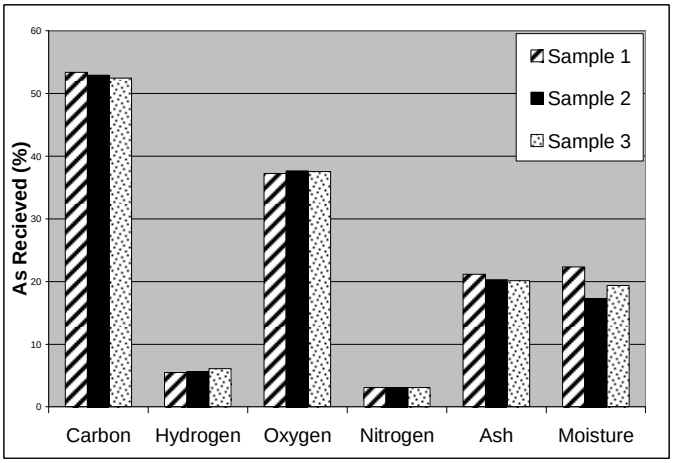

Figure VI.1a: Variation in fuel properties for LAPC biomass

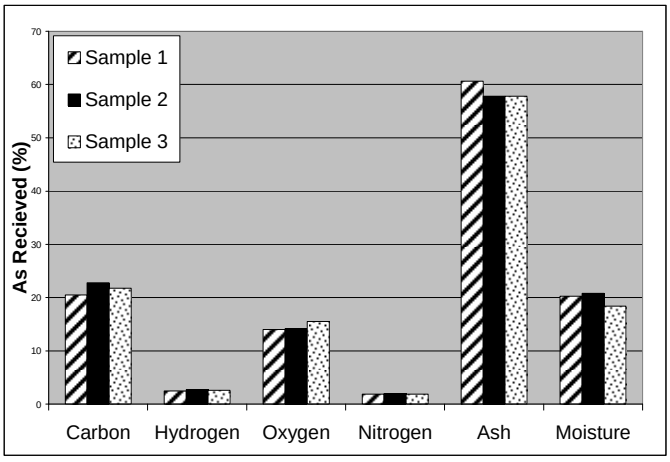

Figure VI.1b: Variation in fuel properties for HARM biomass

A summary of the as received results for the fuels is given in table VI.1. The moisture content of the four biomass fuels is very consistent with an average value of 19.2 %. There is also little variation between the raw manure (RM) samples and the partially composted samples, with the exception of the ash content of the two high ash fuels. The largest difference between the high ash and low ash samples is obviously the ash content. The low ash biomass had an average ash content of 16.3 %, while the ash

content of the high ash biomass averaged 50.5 %. The high ash content presents a major concern for utility application because it could quickly be deposited on heat transfer surfaces inside a utility boiler, reducing the heat transfer rates from gases to water/steam. Texas lignite coal is also listed in the table, but the as received properties of the coal vary greatly from the biomass fuels.

Table VI.1: Ultimate and proximate analysis (As Received)
Note: Average of 3 samples

Ultimate and Proximate Analysis					
As Received (%)					
Fuel	HAPC	LAPC	HARM	LARM	TXL
Proximate:					
Moisture	17.00	19.64	19.81	20.27	38.34
Ash	53.85	16.50	47.10	16.10	11.46
Volatile	25.79	52.33	27.08	51.47	24.79
FC	3.36	11.54	6.02	12.16	25.41
Ultimate:					
Moisture	17.00	19.64	19.81	20.27	38.34
Carbon	14.92	33.79	17.39	34.35	37.18
Hydrogen	1.39	3.65	2.10	4.17	2.12
Nitrogen	1.13	1.97	1.56	2.48	0.68
Sulfer	0.31	0.51	0.34	0.53	0.61
Oxygen	11.40	23.94	11.70	22.10	9.61
Ash	53.85	16.50	47.10	16.10	11.46

To show how similar the biomass samples are and to give a better comparison to coal, the ultimate and proximate analyses are also given on a dry ash free basis, table VI.2. As seen in the table the primary combustion components of the biomass fuels are volatile compounds, > 80 %. HAPC biomass is the only inconsistency on a DAF basis, about 8% higher VM content compared to the other biomasses. There is a large difference between the biomass samples and the coal sample in both VM and FC content. The FC content of TXL coal is just higher than 50 %, indicating it will have a

much higher HHV than the biomass samples, but the FC (char) burns slowly 200 ms to burn a 100 micron char particle. Another meritable difference between the biomass fuels and coal is the oxygen content. The oxygen content of the biomass fuels is ~ 35 – 40 % while the oxygen content of TXL coal is only 20 %. The oxygen content of biomass reduces the HHV due to the presence of oxygenated compounds such as CO, CO_2, and alcohols, etc.

Table VI.2: Ultimate and proximate analysis (Dry Ash Free)
Note: Average of 3 samples

Ultimate and Proximate Analysis					
Dry Ash Free (%)					
Fuel	HAPC	LAPC	HARM	LARM	TXL
Proximate:					
Moisture	0.00	0.00	0.00	0.00	0.00
Ash	0.00	0.00	0.00	0.00	0.00
Volatile	88.47	81.94	81.82	80.89	49.38
FC	11.53	18.06	18.18	19.11	50.62
Ultimate:					
Moisture	0.00	0.00	0.00	0.00	0.00
Carbon	51.19	52.91	52.56	53.99	74.06
Hydrogen	4.77	5.72	6.36	6.55	4.22
Nitrogen	3.87	3.08	4.70	3.90	1.35
Sulfer	1.08	0.79	1.03	0.84	1.22
Oxygen	39.10	37.49	35.35	34.73	19.14
Ash	0.00	0.00	0.00	0.00	0.00

Using the HHV as well as the ultimate and proximate analyses, several combustion properties were calculated (empirical formula, molecular weight of empirical formula, air/fuel ratio, and adiabatic flame temperature under complete combustion), see table VI.3. The HHVs are given on an As Received, Dry, Dry Ash Free, and Volatile Matter basis. On an As Received basis, the low ash biomass fuels have comparable heating values to the Texas lignite coal, while the high ash fuels have a

much lower heating value. Also, the raw manure samples have a higher heating value than the partially composted samples; this is consistent with the findings of Sweeten et al (1990) [1]. Once the moisture is factored out, the similarities between the low ash biomass and TXL coal disappear, with the coal having a much higher heating value. On a dry ash free basis, the high and low ash biomass fuels again show similarities with heating values between 18 and 20 MJ/kg.

Table VI.3: Combustion properties of test fuels
Note: a) Average of 3 samples b) Adiabatic flame temp. based on

Combustion Properties					
Fuel:	HAPC	LAPC	HARM	LARM	TXL
HHV (kJ/kg):					
As Received	5208	13268	6305	13409	14290
Dry	6274	16510	7863	16818	23176
Dry Ash Free	17867	20775	19052	21074	28467
Volatile Matter	15948	18168	16041	18351	24229
Emperical Values:					
Formula					
Carbon	1.00	1.00	1.00	1.00	1.00
Hydrogen	1.11	1.29	1.44	1.44	0.68
Nitrogen	0.06	0.05	0.08	0.06	0.02
Sulfer	0.01	0.01	0.01	0.01	0.01
Oxygen	0.57	0.53	0.50	0.48	0.19
Mol.Wt.	23.5	22.7	22.9	22.2	16.2
$A:F_{stoich.}$	5.87	6.45	6.72	6.97	9.17
Adiabatic Flame Temp. (K)	1202	1407	1165	1341	1378

Table VI.3 also gives empirical values for fuel formula, molecular weight, stoichiometric air/fuel ratio (mass basis), and adiabatic flame temperature. The empirical formulas have been normalized for 1 carbon atom. The stoichiometric air/fuel ratio for coal is much higher than the biomass fuels due in large part to the amount of oxygen already in the biomass fuels. Adiabatic flame temperature is higher for the low

ash fuels compared to the high ash fuels and for partially composted compared to the raw manure samples.

As mentioned in chapter IV, all fuels were sieved prior to testing. The results of the sieve analysis as well as the calculation of Sauter Mean Diameter (SMD) are summarized in table VI.4. In addition, the Rosin Rammler distributions are plotted in figure VI.2. The results show similarities between the raw and partially composted biomass samples; however, there are large differences for SMD between the high and low ash samples. This is most likely due to the size of the ash particles. The ash is related to the surface of the feedlot, and in the high ash case, it is directly related to the soil in the area of the feedlot. The major soil component in the Amarillo area is Pullman clay loam which has an SMD of 3 microns. It should be noted that the kinetics and ignition results assume spherical geometries for the particles for calculation purposes; however, theses particles could be fibrous or elongated. This would artificially increase the particles in the larger size classifications.

Table VI.4: Sieve results and SMD for all fuels
Note: Average of 3 samples

Particle Size Distribution					
Mean Dia. (μm)	**HARM** (%)	**LARM** (%)	**HAPC** (%)	**LAPC** (%)	**TXL** (%)
1596	0.02	0.05	0.02	0.06	0.00
1015	0.03	0.06	0.05	0.11	0.00
570	2.73	10.81	2.40	7.79	5.23
225	8.96	24.50	7.92	27.25	35.38
113	17.16	22.55	15.42	22.98	35.02
60	21.00	15.35	20.03	15.36	11.62
22.5	50.09	26.68	54.15	26.44	12.75
SMD (μm)	36.12	56.54	34.37	56.51	80.88

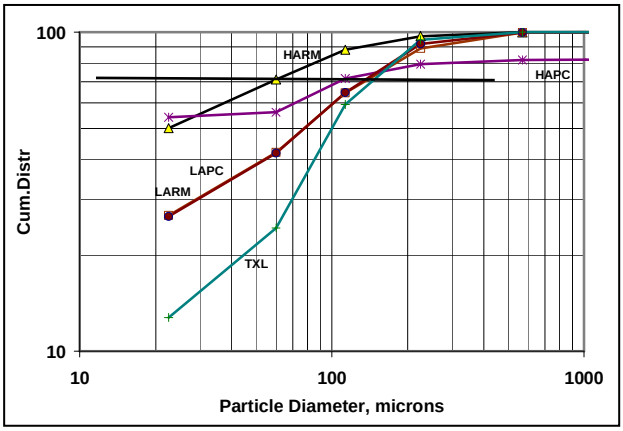

Figure VI.2: Rosin Rammler distribution of samples

VI.3 Single Reaction Model

In chapter V, three single reaction model solutions were described for calculating the activation energy and pre-exponential factor, method A: slope approximation, method B: rigorous solution, and method C: maximum volatile release rate. The slope approximation results are discussed first, followed by the rigorous solution results, and finally the maximum volatile release rate results.

Method A: Slope Approximation

As mentioned earlier, the slope approximation is only valid for test results where the expression $E/\overline{R}T$ is between 20 and 60. None of the samples tested fell into the valid range for this expression; however, the results for pure samples of each fuel are presented in Figure VI.3 for brief discussion. The results indicate that the activation energy for low ash biomass is higher than that of high ash biomass for both raw and partially composted samples. Also, the raw manure samples have slightly higher activation energies than the partially composted samples. It is noted that a uniform particle temperature assumption has been used. The size effect on pyrolysis values

comes through the temperature gradient within the particle; however, the particle sizes here are extremely small. In addition, the heating rates are low; thus, the size effect may not be responsible for different activation energies. The results also show the activation energy for Texas lignite coal to be lower than all four types of biomass, a result that is counter to results observed in the literature review [11, 12]. Again, the significance of these results is questionable since the validation for using the slope approximation failed. It should be noted that the two constants in the slope approximation formula, equation (V.7) can be adjusted to better fit the data; however, once adjusted the valid range for the formula would be unknown.

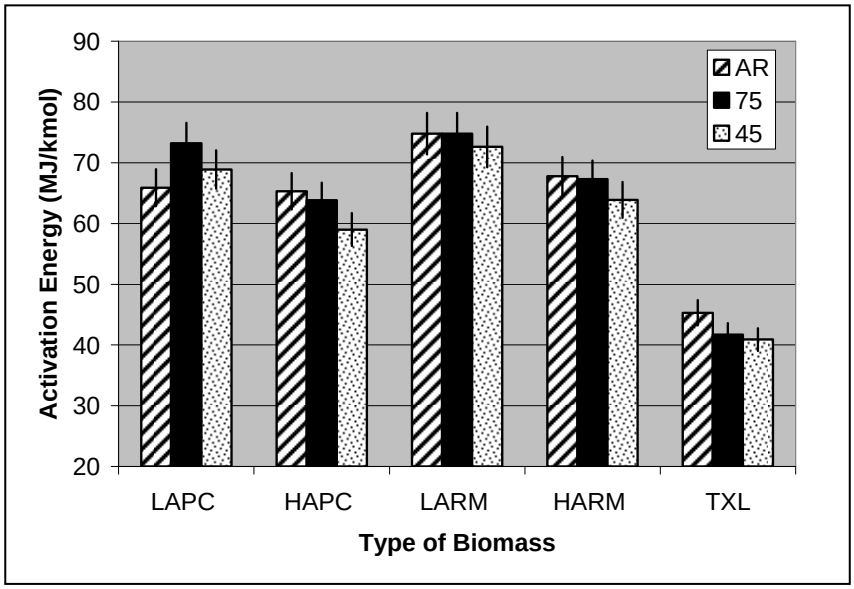

Figure VI.3: Activation energy results obtained using the slope approximation

Method B: Rigorous Solution

The differences between the two solution methods can be observed graphically, see figure VI.4. In the figure, the slope approximation and the rigorous solution are

compared to the original thermogram measured in the TGA. Over the range of primary volatile loss, points in white, the rigorous solution shows a better fit for the data.

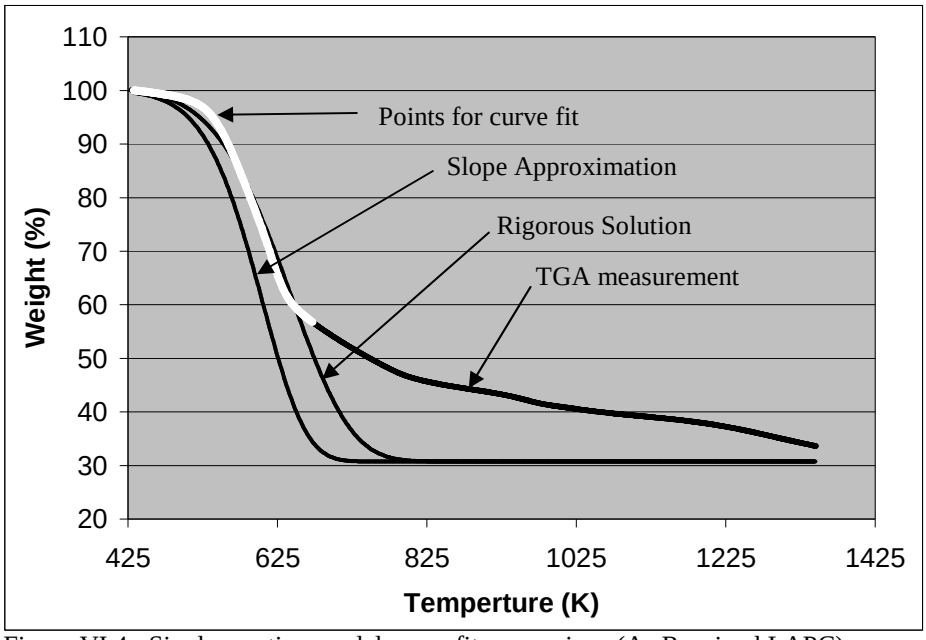

Figure VI.4: Single reaction model curve fit comparison (As Received LAPC)

Detailed results for the rigorous solution are discussed first by comparing all four biomass fuels at various blend ratios with Texas lignite coal, and second, the individual biomass fuels are analyzed for differences in activation energy based on particle size. Figures VI.5a, b, c give the activation energy results for the biomass fuels for as received (AR), 60 μm, and 22.5 μm particle sizes respectively.

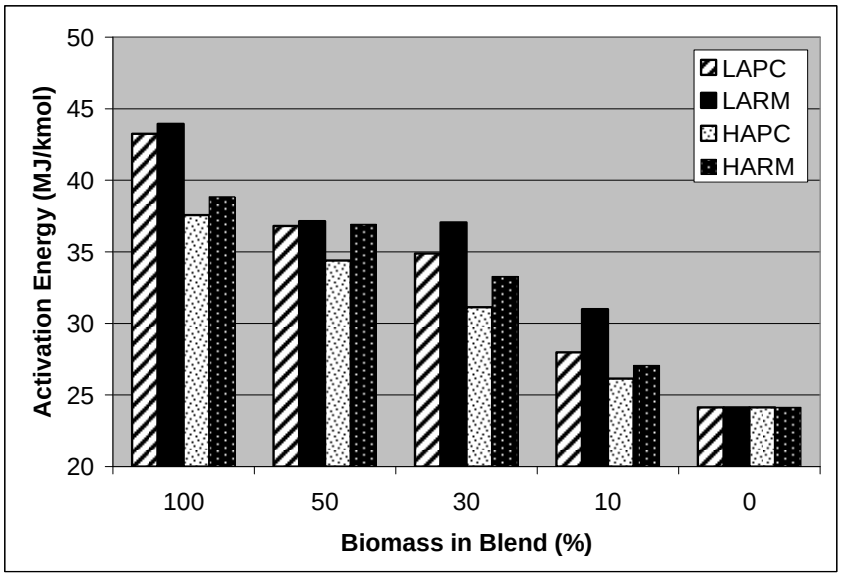

Figure VI.5a: Single reaction model rigorous solution activation energy for as received classification

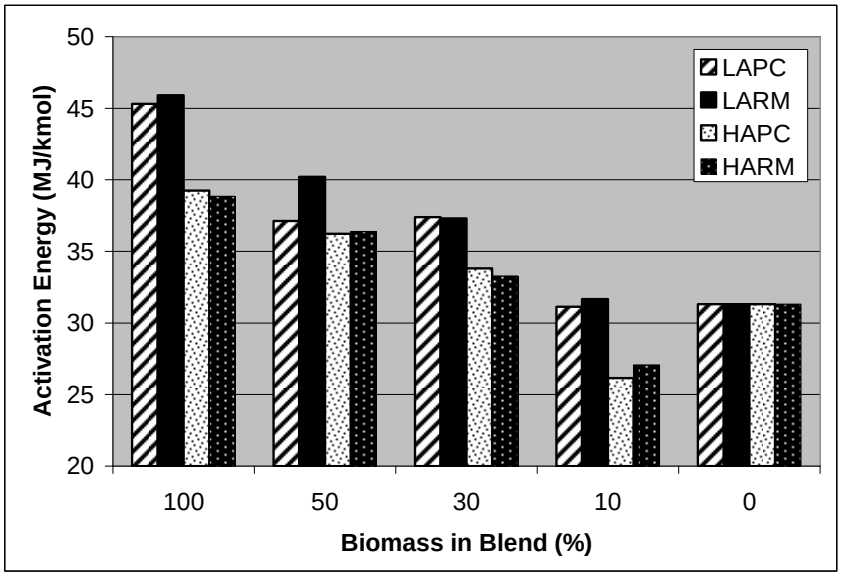

Figure VI.5b: Single reaction model rigorous solution activation energy for 60 μm classification

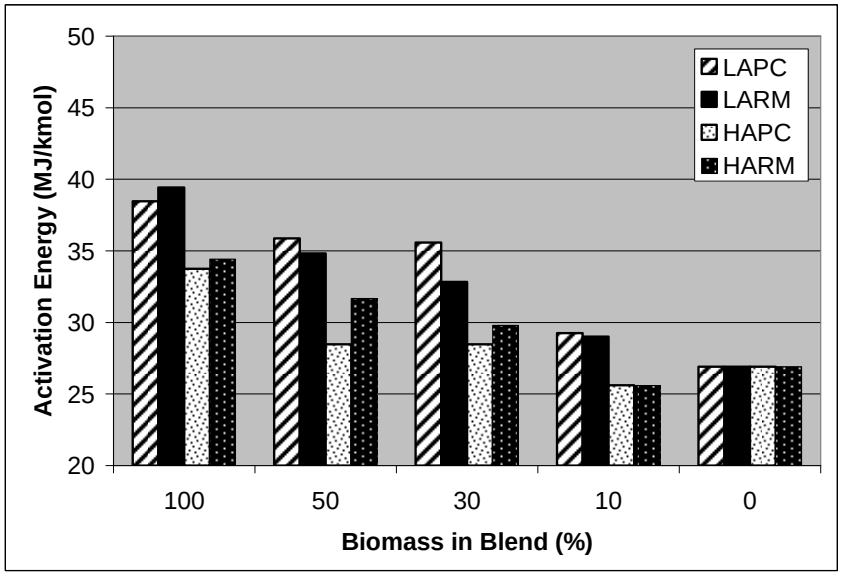

Figure VI.5c: Single reaction model rigorous solution activation energy for 22.5 μm classification

The results show that in general the activation energy decreases with increasing coal in the blend. As with the slope approximation, the raw manure samples tend to have higher activation energies than the partially composted samples. In addition, the high ash samples generally have lower or equivalent activation energy when compared to the low ash samples, indicating that the ash in the sample tends to lower the activation energy.

The data in figures VI.5a, b, c are regrouped by type of biomass to show a comparison based on particle size in figures VI.6a, b, c, d.

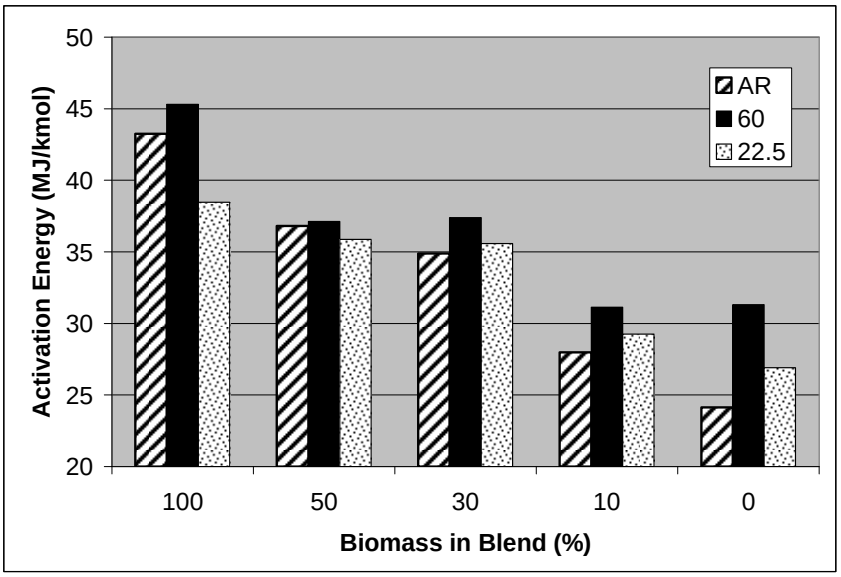

Figure VI.6a: Single reaction model rigorous solution activation energy for LAPC biomass, effect of particle size

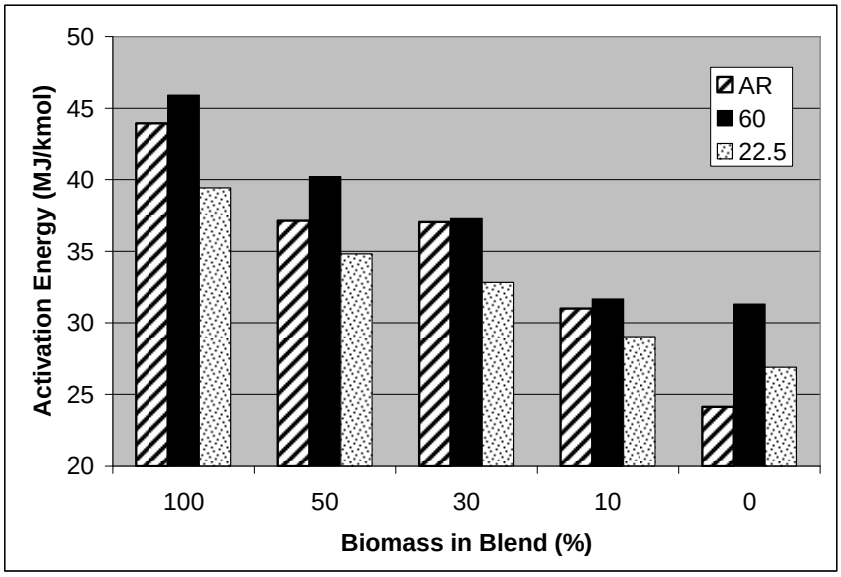

Figure VI.6b: Single reaction model rigorous solution activation energy for LARM biomass, effect of particle size

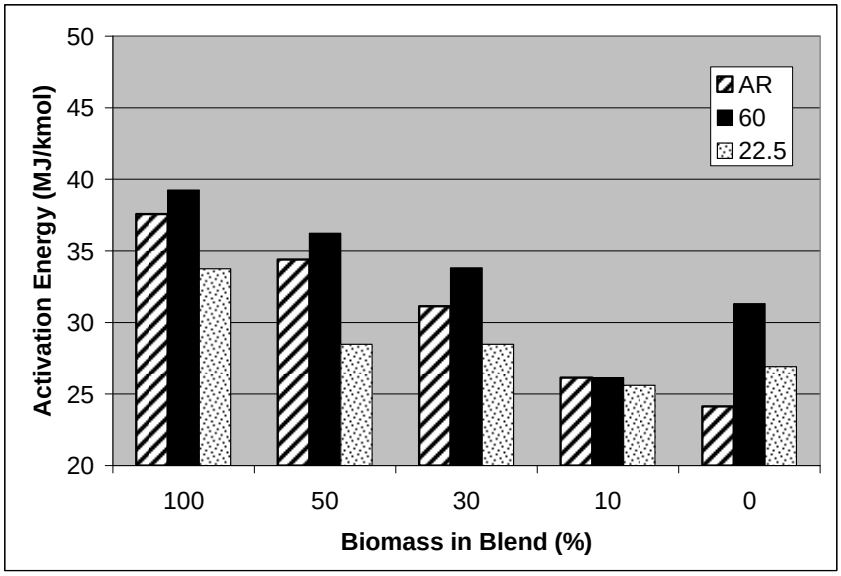

Figure VI.6c: Single reaction model rigorous solution activation energy for HAPC biomass, effect of particle size

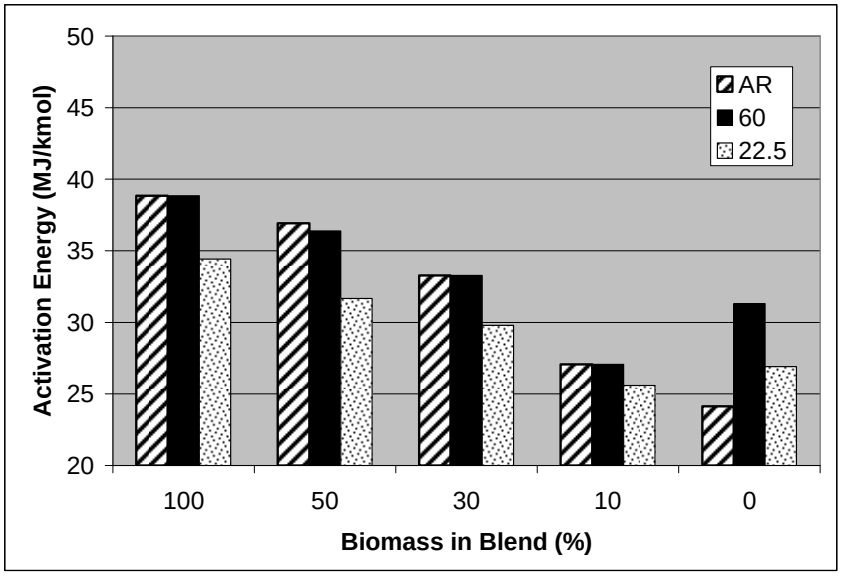

Figure VI.6d: Single reaction model rigorous solution activation energy for HARM biomass, effect of particle size

In all cases (pure biomass, pure coal, and blends) except the HARM, the activation energies for the 60 micron particle size group are higher than the as received

particle size group. This is most likely due to the fixed carbon content of the samples. The HARM sample also had a lower dry ash free fixed carbon content compared to the other three biomass fuels. The activation energy for the 22.5 micron particle group is generally lower than the other two size classes for all four fuels. Also, the ash content of this size class is higher than the others as a result sieving as discussed earlier. This supports the case that higher ash content tends to lower the activation energy of the fuel.

The frequency factor was also calculated for each of the samples tested; however, the values were not consistent with the state theory assumption of 1.67E+13 s^{-1}. In most cases the frequency factor was below 500 s^{-1} with a maximum value of 2800 s^{-1}. Figure VI.7 shows the effect of fixing the frequency factor at 1.67E+13 s^{-1} for the single reaction model. The results indicate that although fixing the frequency factor is more consistent with theory, allowing it to vary gives a better fit of the data.

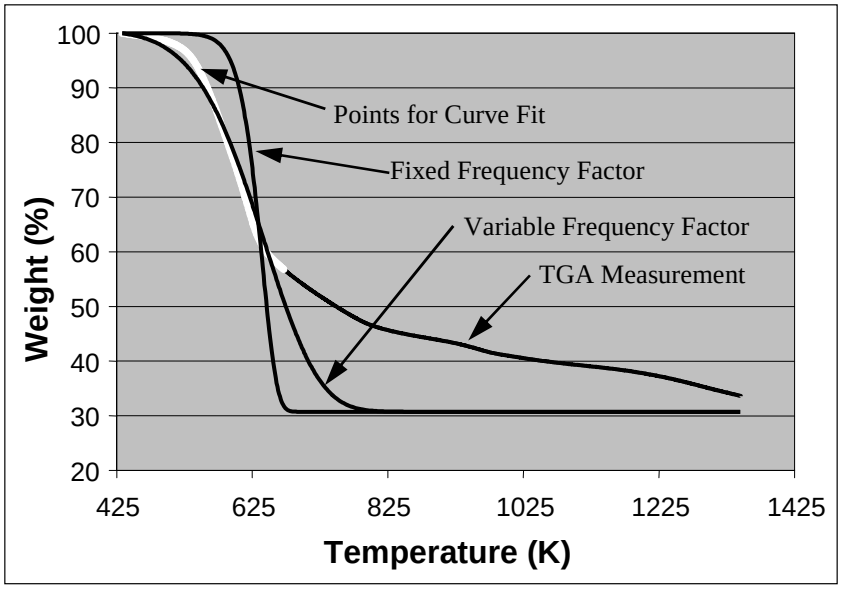

Figure VI.7: Comparison of fixed vs. variable frequency factor for the single reaction model

Method C: Maximum Volatile Release Rate

The results obtained for the MVRR method are summarized in table (VI.5). Temperatures are various stages of pyrolysis are also given in the table, (10%, 50%, and 80% volatile loss). The results show some correlation with the other single reaction models for the low ash samples, and less correlation for the high ash samples. Biomass fuels and coals are heterogeneous by nature, with volatile compounds releasing at different temperatures. The results of the MVRR model would likely be better for a homogeneous sample.

Table VI.5 Single reaction model method C: MVRR results and pyrolysis temperatures
Note: Average of 2 trials

Pyrolysis Properties					
Fuel:	HAPC	LAPC	HARM	LARM	TXL
Pyrolysis Temeperature (K)					
T (10% loss)	570	550	560	550	620
T (50% loss)	820	630	740	620	820
T (80% loss)	1290	890	1260	820	1070
Single Reaction Model: Maximum Volatile Release Rate					
dm/dt max %/K)	-0.36	-0.62	-0.41	-0.62	-0.28
mv (dm/dt max) (%)	75	55	70	52	68
T (dm/dt max) (K)	620	620	620	620	740
Activatioin Energy (kJ/mol)	15200	35900	18900	37800	18600
Frequency Factor (1/s)	0.062	8.241	0.155	12.476	0.057

VI.4 Distributed Activation Energy Model

The results for the distributed activation energy model (DAEM) are discussed first by comparing all four fuels at various blend ratios with Texas lignite coal (TXL), figures IV.8a,b; 9a,b; and 10a,b. In the figures, "*a*" denotes the activation energy chart, and "*b*" denotes the standard deviation of the activation energy.

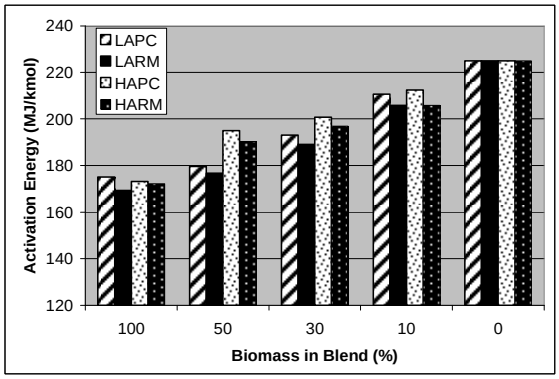

Figure VI.8a: DAEM activation energy of as received biomass fuels

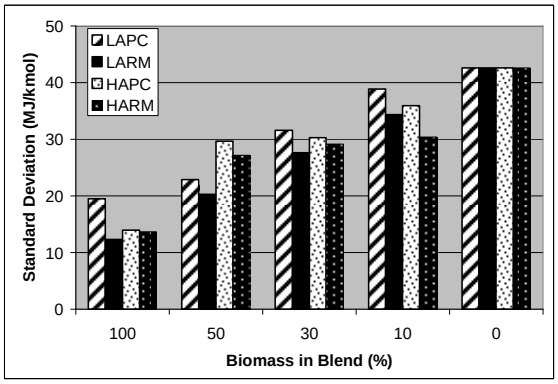

Figure VI.8b: DAEM standard deviation of as received biomass fuels

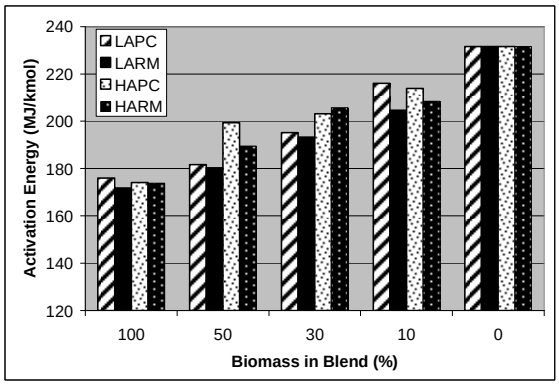

Figure VI.9a: DAEM activation energy of 60 micron class biomass fuels

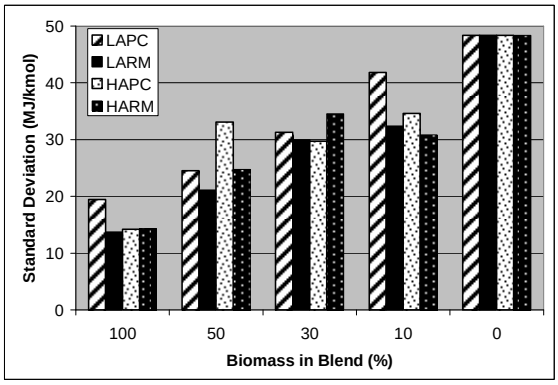

Figure VI.9b: DAEM standard deviation of 60 micron class biomass fuels

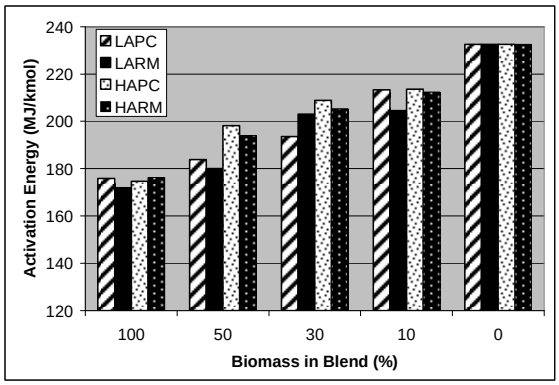

Figure VI.10a: DAEM activation energy of 22.5 micron class biomass fuels

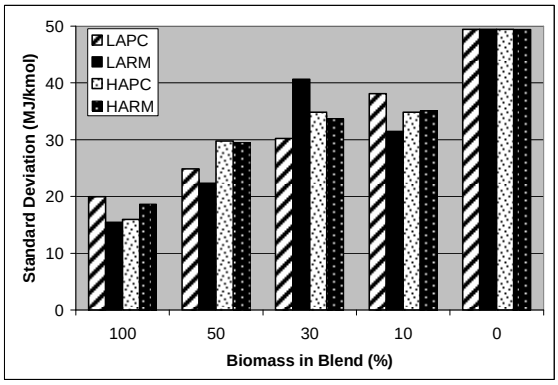

Figure VI.10b: DAEM standard deviation of 22.5 micron class biomass fuels

The average activation energies were 174 (kJ/mol) for feedlot biomass and 230 (kJ/mol) for Texas lignite coal. These values are very consistent with results from literature. In all cases, the activation energy increases as the amount of coal in the blend increases. However, the relationship between activation energy and blend ratio is nonlinear as seen in figure VI.11; a linear relationship would indicate a direct relation to mass.

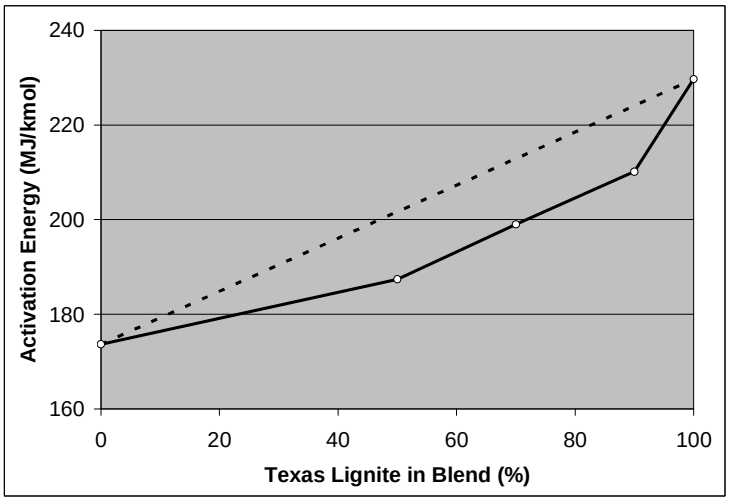

Figure VI.11: Average activation energy of biomass fuels for DAEM as a function of TXL coal percentage in blend

The relationship between blend ratio and activation energy can be modeled by the following series of equations:

$$\frac{dm_v}{dt} = -\left[k_c \cdot \exp\left(-\frac{E_c}{\overline{R}T} \right) \cdot m_{v,c} + k_b \cdot \exp\left(-\frac{E_b}{\overline{R}T} \right) \cdot m_{v,b} \right] \qquad \text{(a)}$$

Where the subscripts "*c*" and "*b*" designate coal and biomass respectively

$$\begin{aligned} m_{v,c} &= m \cdot Y_{c,blend}(VM_c) \\ m_{v,b} &= m \cdot Y_{b,blend}(VM_b) \end{aligned} \qquad \text{(b)}$$

$$\frac{dm_v}{dt} = -m \cdot \left[k_c \cdot \exp\left(-\frac{E_c}{\overline{R}T} \right) \cdot Y_{c,blend}(VM_c) + k_b \cdot \exp\left(-\frac{E_b}{\overline{R}T} \right) \cdot Y_{b,blend}(VM_b) \right] \qquad \text{(c)}$$

Since E_c, E_b, $(VM)_c$, and $(VM)_b$ are different, one would not expect a linear relation.

The activation energies for the high ash biomass fuels tend to be higher in almost all cases. The only exceptions are the pure samples of partially composted biomass. Also, in general the partially composted samples have higher activation energies than the raw manure samples.

The trends for the standard deviations are similar to those found in the activation energies. As the amount of Texas lignite coal in the blend increases, the standard deviation also increases. The standard deviation is also higher for the partially composted samples compared to the raw manure samples; however, the standard deviation data is a bit more scattered and more exceptions are present. There is no discernable overall trend relating the high and low ash samples. In all the 50-50 blends, the high ash samples have a higher standard deviation, while in the 90-10 blends the low ash samples have a higher standard deviation. All of the results obtained thus far for the distributed activation energy model are in direct contrast to the results of the single reaction model. This will be discussed in greater detail later in the section.

Next, the fuels are individually compared based on particle size, figures VI.12a,b; 13a,b; 14a,b; and 15a,b. As before, the subscripts with "*a*" denote the activation energy chart, and "*b*" denote the standard deviation of the activation energy chart.

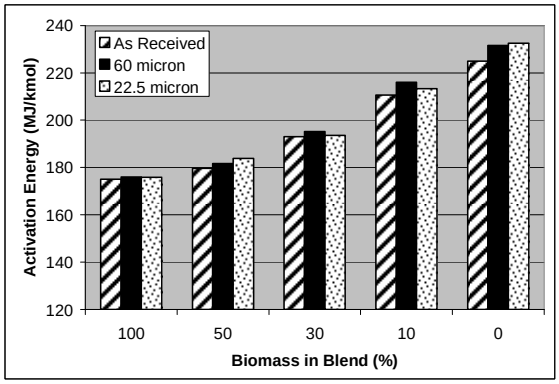

Figure VI.12a: DAEM activation energy of LAPC biomass

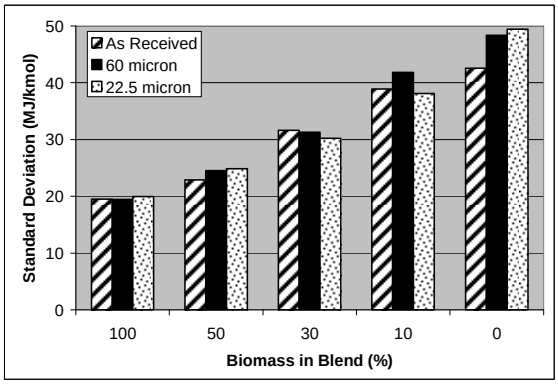

Figure VI.12b: DAEM standard deviation of LAPC biomass

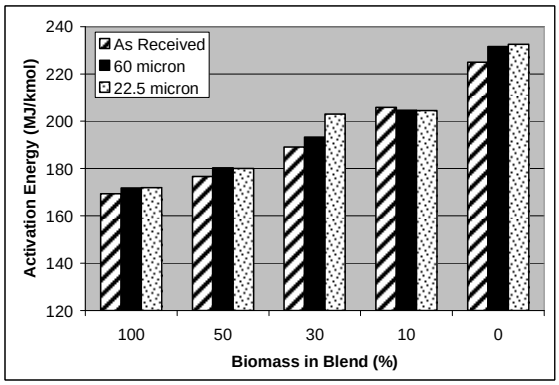

Figure VI.13a: DAEM activation energy of LARM biomass

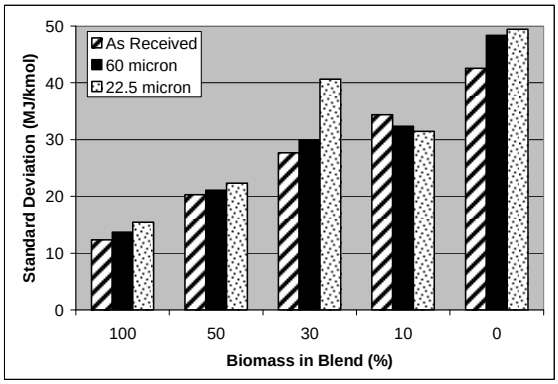

Figure VI.13b: DAEM standard deviation of LARM biomass

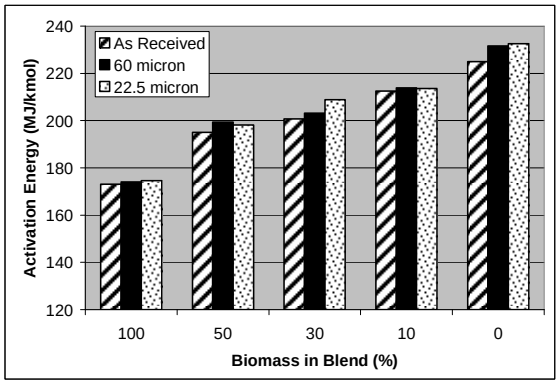

Figure VI.14a: DAEM activation energy of HAPC biomass

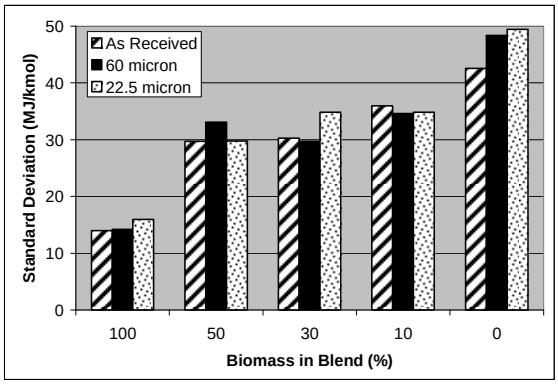

Figure VI.14b: DAEM standard deviation of HAPC biomass

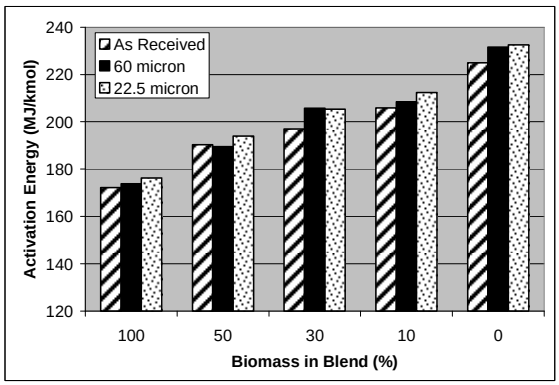

Figure VI.15a: DAEM activation energy of HARM biomass

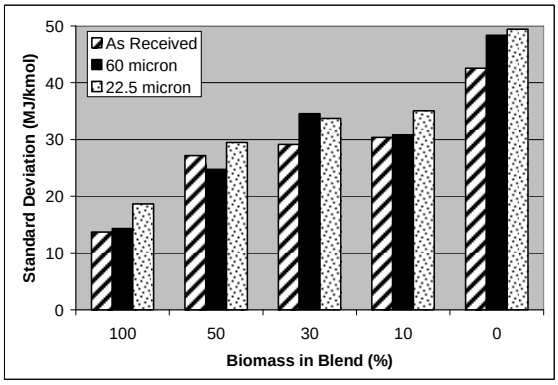

Figure VI.15b: DAEM standard deviation of HARM biomass

For the pure biomass samples, there is very little change in activation energy with respect to changes in particle size, with the 22.5 micron classification having only slightly higher activation energies. The three blended cases show that the activation energy increases as the particle size decreases. As mentioned in previous chapters it is likely that the percentage of ash in the smaller particle size classes is higher than for the as received samples since the ash particles are very small, indicating the activation energy is higher for samples with higher ash content. This result is supported by the results that showed the high ash biomass samples to have higher activation energy than the low ash samples unless catalytic effects are present. Higher ash can slow the flow of volatiles thereby increasing the "apparent" activation energy. Again, these trends are opposite the trends observed in the single reaction model results. Out of the 13 different comparisons of standard deviation change with respect to particle size, 6 show an increase in standard deviation for the 60 micron size class over the as received class, 4 show relatively little change, and 3 show a decrease. However, 10 of the 22.5 micron

samples show an increase in standard deviation compared to the as received size class; this may be due to large ash content variation.

Since the results of the distributed activation energy model and the single reaction model tend to be in direct contrast, some discussion is warranted. Both calculations use an iterative process to arrive at the solution. The solution is determined by minimizing the squared error between the measured and theoretical thermograms. The average values for the squared error are as follows: SRM 0.90, DAEM 0.37. Table VI.6a,b give the average squared errors for the single reaction model rigorous solution grouped by fuel ratio and particle size respectively. The same information is given for the distributed activation energy model in Table VI.7a,b. The SRM data shows that the high ash calculations more closely followed the data than did the low ash samples. The error also decreases with increased coal in the blend. Smaller particle sizes showed decreased error as well. The trends are not as apparent in the DAEM error results. The high ash samples did have lower errors, but the differences are not as large as those for the SRM. This implies that the DAEM model is much more applicable for different types of fuels. Also, the DAEM model uses a fixed value for frequency factor of 1.67E+13 s^{-1} obtained from the literature; whereas, the SRM allows this value to vary. However, the frequency factors obtained using the SRM were not consistent with the theoretical value. Finally, modeling results from the overall research project at Texas A&M University show that the activation energies obtained using the DAEM are more applicable.

Table VI.6a: Average summed error for the single reaction model grouped by fuel ratio

Biomass in Blend	LAPC	HAPC	LARM	HARM
100	5.638	0.572	6.559	0.966
50	1.439	0.037	1.722	0.124
30	0.257	0.007	0.439	0.019
10	0.011	0.014	0.039	0.010
0	0.047	0.047	0.047	0.047

Table VI.6b: Average summed error for the single reaction model grouped by particle size

Particle Size	LAPC	HAPC	LARM	HARM
AR	1.824	0.174	2.144	0.330
60	1.467	0.170	1.570	0.216
22.5	1.144	0.063	1.569	0.153

Table VI.7a: Average summed error for the distributed activation energy model grouped by fuel ratio

Biomass in Blend	LAPC	HAPC	LARM	HARM
100	0.693	0.194	0.314	0.304
50	0.537	0.305	0.504	0.326
30	0.364	0.180	0.452	0.247
10	0.282	0.235	0.282	0.181
0	0.482	0.482	0.482	0.482

Table VI.7b: Average summed error for the distributed activation energy model grouped by particle size

Particle Size	LAPC	HAPC	LARM	HARM
AR	0.465	0.272	0.373	0.283
60	0.525	0.323	0.413	0.314
22.5	0.426	0.243	0.434	0.327

VI.5 Ignition

The ignition temperature results are grouped similarly to the activation energy results, discussing the effect of different types of biomass first followed by a discussion of particle size effects.

Effect of Fuel

Figures VI.16a, b, c compare the ignition temperature results of the different types of biomass. The results indicate that the presence of coal in the sample has a the greatest effect on the ignition temperature compared to other variables. The average ignition temperature of all samples with coal was 577 K (high: 611 K, low: 555 K, σ: 2.6%). While the samples without coal had an average ignition temperature of 744K (high: 790 K, low: 727 K, σ: 2.2%). In several of the blended samples the high ash samples had a higher ignition temperature than the low ash samples. This trend is not observed in the pure biomass samples. For the as received and 60 micron particle size groupings, the high ash partially composted sample had the higher ignition temperature, while in those same classes the low ash raw manure had the higher ignition temperature.

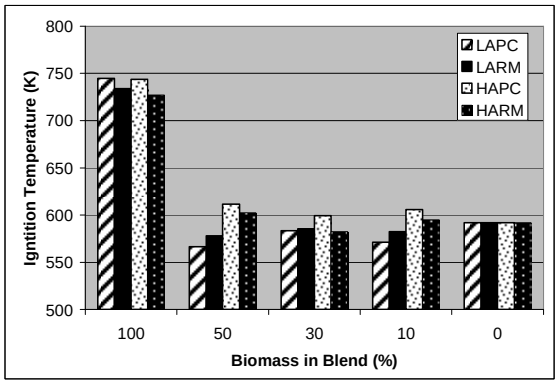

Figure VI.16a: Ignition temperatures for the as received particle class

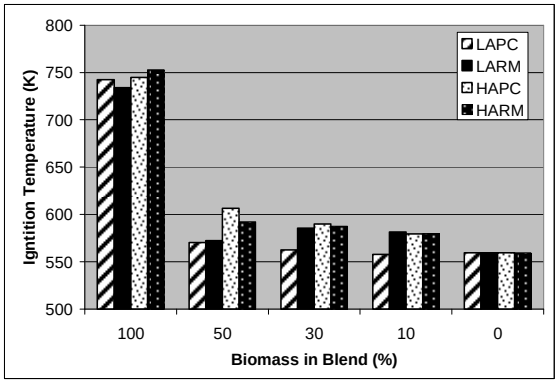

Figure VI.16b: Ignition temperatures for the 60 micron particle class

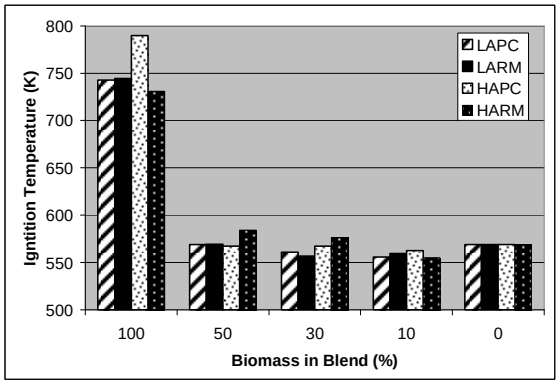

Figure VI.16c: Ignition temperatures for the 22.5 micron particle class

Effect of Particle Size

The effect of particle size on ignition temperature can be seen in figures VI.17a, b, c, d. For the low ash samples the ignition temperature of the as received particle size group is noticeably higher than the other two classifications at blend percentages less than 30%. This result is also seen in the pure Texas lignite sample. For the high ash samples, the as received particle size group has a higher ignition temperature for all but one of the blended samples. There is no distinguishable effect of particle size on pure biomass ignition temperature.

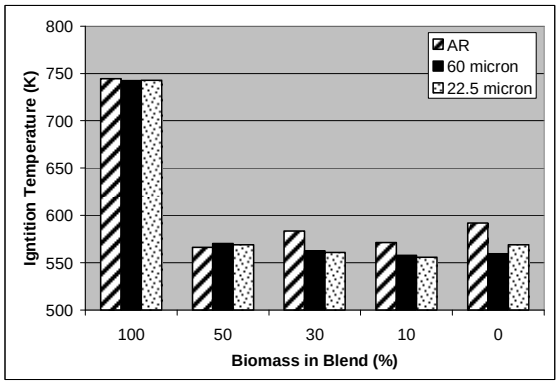

Figure VI.17a: Ignition temperatures for LAPC biomass

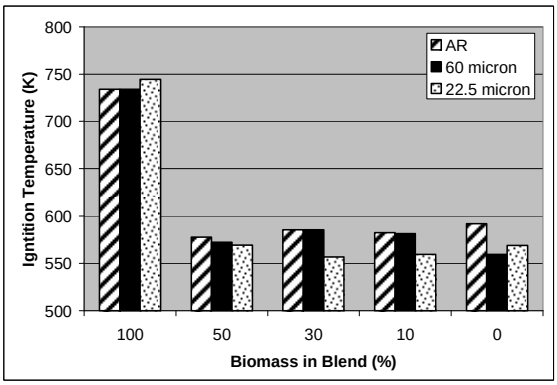

Figure VI.17b: Ignition temperatures LARM biomass

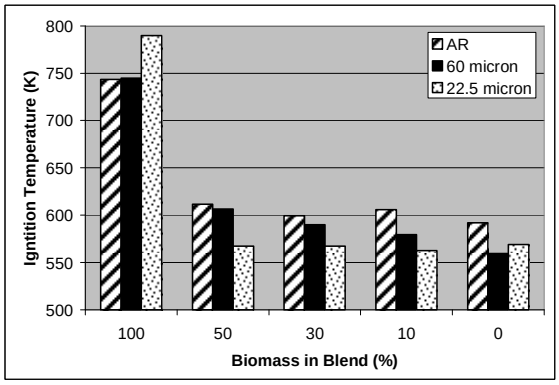

Figure VI.17c: Ignition temperatures for HAPC biomass

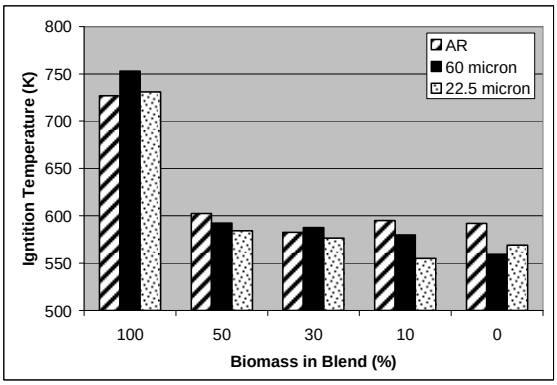

Figure VI.17d: Ignition temperatures for HARM biomass

Finally, table VI.8 gives a comparison of pyrolysis and ignition temperature found for each of the pure fuels. The data clearly show that for biomass fuels ignition occurs during pyrolysis, after 50% loss in three of the four cases. However, for the TXL sample, ignition during the beginning stages of pyrolysis.

Table VI.8: Pyrolysis/Ignition temperature comparison
Note: Average of 2 samples

Pyrolysis/Ignition Temperature Comparison					
Fuel:	HAPC	LAPC	HARM	LARM	TXL
Temeperature (K)					
T (10% loss)	570	550	560	550	620
T (50% loss)	820	630	740	620	820
T (80% loss)	1290	890	1260	820	1070
T (dm/dt max)	620	620	620	620	740
T (ignition)	744	745	727	746	592

CHAPTER VII

CONCLUSIONS

Several conclusions can be drawn from the results obtained for feedlot biomass.

1. All three single reaction models (slope approximation, rigorous solution, and maximum volatile rate) yield a lower value for activation energy for lignite, biomass, and blends compared to the distributed activation energy model.
2. The distributed activation energy model provides more applicable results than the single reaction model for the pyrolysis behavior of feedlot biomass and blends of feedlot biomass with coal. This statement is supported by the wide use of the distributed activation energy model to study the behavior of non-uniform solid fuel particles as observed in the literature and the comparability of these results to literary results.
3. The relative accuracy of the distributed activation energy model is better since the average error was smaller.
4. The increased ash content of the biomass tends to increase the activation energy required for combustion of biomass fuels. This is observed directly in the calculation of activation energy using the distributed activation energy model.
5. While initial observation suggests that particle size tends to increase activation energy, the increased activation energy is more likely a result of increased ash content in the smaller sample sizes. Performing ultimate and proximate analysis on the sieved samples could confirm this hypothesis.

6. The ignition temperature results indicate that biomass fuels ignite at higher temperatures than coal despite the fact that biomass pyrolysis has lower activation energy. It is theorized that the increased volatile content of biomass fuels carries away a portion of the heat required for biomass ignition thereby delaying the onset of ignition as outlined in the literature review.

CHAPTER VIII

RECOMMENDATIONS

Recommendations for future work in this area include:

1. Perform the ultimate and proximate analysis on the sieved samples of each fuel to determine what affect this has on sample composition.
2. Conduct experiments on samples with like composition but with varied particle size to isolate this variable.
3. Repeat experiments on dairy biomass and compare results
4. Efforts were made to store the samples in sealable containers; however, moisture content of the samples changed by a factor of ½ during storage. While this did not seem to affect the pyrolysis or ignition results, future samples should be stored in moisture tight containers to ensure consistency in samples using a controlled humidity chamber.
5. Re-evaluate data using two reaction models, one for the region of primary loss, and one for the region of secondary loss.

REFERENCES

[1] Sweeten JM. Cattle feedlot waste management practices for water and air pollution control. Texas Agricultural Extension Service. 1990;Pub B-1671.

[2] Miles TR, Baxter LL, Bryers RW, Jenkins BM, Oden LL. Alkali deposits found in biomass power plants a preliminary investigation of their extent and nature. National Renewable Energy Laboratory. 1995.

[3] Young L, Pian C. High temperature air blown gasification of dairy farm wastes for energy production. Energy. 2003;28:655-672.

[4] Miller BG, Miller SF, Scaroni AW. Utilizing agricultural by-products in industrial boilers: Penn state's experience and coal's role in providing security for our nation's food supply. 19th Annual International Pittsburgh Coal Conference. 2002.

[5] Thien B. Cofiring with coal-feedlot biomass blends. Doctoral dissertation. Texas A&M University. College Station, Texas. 2002.

[6] Annamalai K, Thien B, Sweeten J. Co-firing of coal and cattle feedlot biomass (FB) fuels Part II Performance results from 30 kW (100,000) BTU/h laboratory scale boiler burner. Fuel. 2003;82:1183-93.

[7] Park TJ, Kim JH, Lee JG, Hong JC, Kim YK, Choi YC. Experimental Studies on the Characteristics of Entrained Flow Coal Gasifier. 13th U.S.-Korea Joint Workshop on Energy and Environment. 1999.

[8] Fryda L, Panopoulos K, Vourliotis P, Pavlidou E, Kakaras E. Experimental investigation of fluidized bed co-combustion of meat and bone meal with coals and olive bagasse. Fuel 2006;85:1685-1699.

[9] Annamalai K, Puri IK. Combustion science and engineering 1st ed Orland, FL: Taylor and Francis; 2005 Ch. 5.

[10] Dutta S, Wen CY Belt RJ. Reactivity of coal and char in carbon dioxide atmosphere. Industrial & Engineering Chemistry Process Design and Development. 1977;16:20-30.

[11] Anthony DB, Howard HC, Hottel HC, Meissner HP. Rapid devolatilization of pulverized coal. Symposium (International) on Combustion. 1974;15:1303-1317.

[12] Raman P, Walawander WP, Fan LT, Howell JA, Thermogravimetric analysis of biomass devolatilization studies on feedlot manure. Industrial & Engineering Chemistry Process Design and Development. 1981;20:630-640.

[13] Annamalai K, Ryan W, Dhanapalan S. Interactive processes in gasification and combustion -Part III: coal/char particle arrays, streams and clouds. Progress in Energy and Combustion Science. 1995;20:487-618.

[14] Donskoi E, McElwain DLS. Approximate modeling of coal pyrolysis. Fuel 1999;78:825-835.

[15] Donskoi E, McElwain DLS. Optimization of coal pyrolysis modeling. Combustion and Flame 2000;122-3:359-367.

[16] Please CP, McGuinness MJ, McElwain DLS. Approximation to the distributed activation energy model for the pyrolysis of coal. Combustion and Flame 2003;133:107-117.

[17] Jinno D, Gupta AK, Yoshikawa K, Determination of chemical kinetic parameters of surrogate solid waste. Journal of Engineering for Gas Turbines and Power. 2004;126:685-692.

[18] Tognotti L, Malotti A, Petarca L, Zanelli S. Measurement of ignition temperature of coal particles using a thermo gravimetric technique. Combustion Science and Technology. 1985;44:15-28.

[19] TA Instruments Q Series™ Thermal Analyzers. TA Instruments Internal Publication. SDT 47-53.

APPENDIX A

Principle of Operation for TGA

The TA Instruments Q600 thermogravimetric analyzer uses an accurate and highly reliable horizontal dual-balance mechanism that supports both DSC and TGA measurement. The sample balance monitors actual sample weight, while the reference balance is used to correct the TGA measurement for beam growth. The dual-beam design results in less drift compared to single-beam designs, improving accuracy and precision. During testing, the test sample is placed in an alumina sample pan, which in turn rests on the sample balance beam. A thin layer of alumina powder separates the sample pan from the thermocouples. A matched platinum/platinum rhodium thermocouple pair embedded in the ceramic beams provides sample, reference, and differential temperatures from ambient up to 1500 C. Temperatures are maintained by an ultra-reliable bifilar-wound furnace. The furnace is capable of heating rates up to 100 C/min, and software available for the Q600 allows the user to change the heating rate, hold at constant temperature, or any combination of the two. The Q600 also features a horizontal purge gas system with digital mass flow controllers and gas switching capability. Accurately metered gas flows through the furnace and directly across the sample and reference pans prior to exiting the analyzer. The exit port can also directly interface a mass spectrometer or FTIR.[19]

VITA

Name: Brandon Ray Martin

Address: 2495 South Mason Rd. Apt. 1134, Katy, TX, 77450

Email Address: brm777@tamu.edu

Education: B. S. Mechanical Engineering, University of Arkansas, May 2003
M. S. Mechanical Engineering, Texas A&M University, Dec. 2006